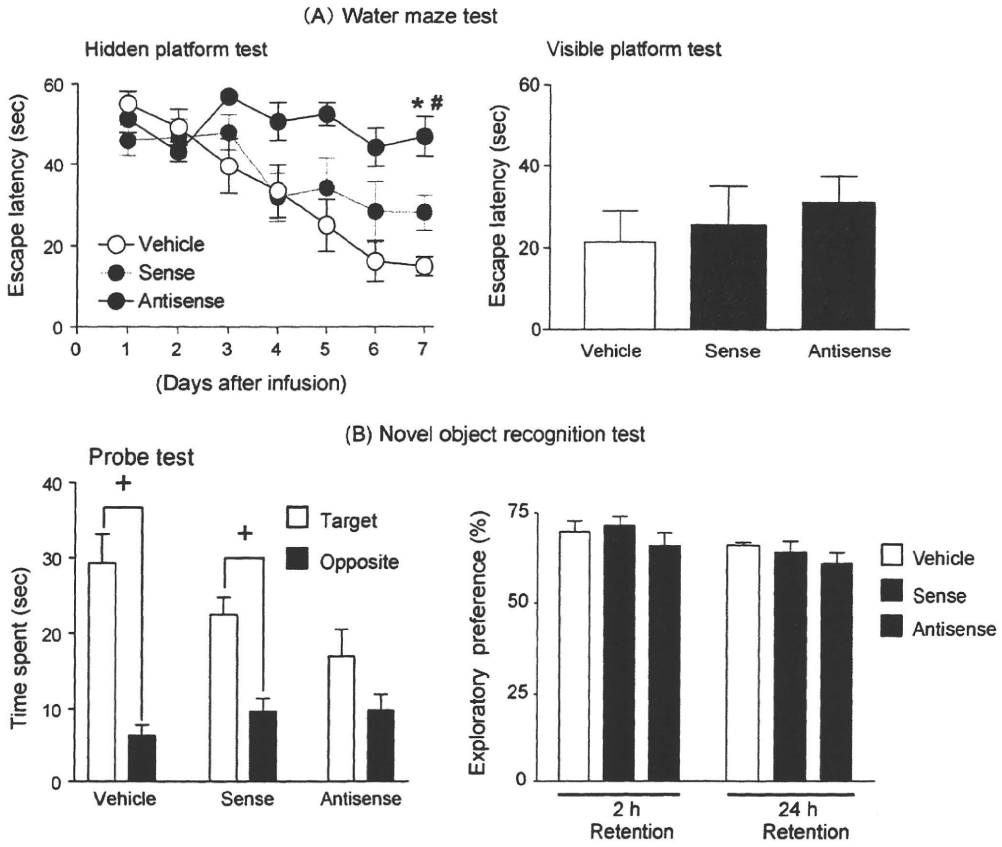

Fig. 2. Effect of Piccolo antisense injection on spatial learning and recognition memory. The hidden platform test in the Morris water maze began 24 h after the infusion (A). Escape latency for the animals in the hidden (left) and visible (right) platform tests was shown. Cut off time was 60 s. Time spent in target and opposite quadrants in the probe test was also showed (left below). Each value represents the mean ± SEM for 8–9 experiments. $^{*}p < 0.05$ vs. vehicle-treated mice. $\#p < 0.05$ vs. sense-treated mice. $+p < 0.05$ vs. target quadrant in each group. Effect of down-regulation of Piccolo expression by antisense injected into the ventricle on performance in a novel object recognition test (B). Recognition memory in the novel object recognition test was not impaired by infusion of Piccolo antisense into the ventricle. The time spent exploring two objects was measured for 10 min during training. Retention sessions were performed either 2 h or 24 h after the training session. Each value represents the mean ± SEM for 7 experiments.

learning and memory. Thus, we investigated the effect of Piccolo antisense on baseline response and LTP in these subregions by using simultaneous recording from a hippocampal slice with a MED system. In area CA1, vehicle- and sense-treated groups exhibited stable LTP whereas the Piccolo antisense-treated group displayed a lower level of LTP (Fig. 3A and B). In contrast, in the DG there was no significant difference in LTP among Piccolo sense-, antisense- and vehicle-treated mice (Fig. 3C and D). Piccolo sense and antisense infusions did not affect baseline response in either subregion (Fig. 3A and C). These results suggest a requirement for a normal Piccolo level for the proper expression of LTP in area CA1 but not in the DG.

3.4. Effect of Piccolo antisense injection on PPF in area CA1

We investigated the effect of Piccolo antisense on PPF to determine whether pre- or post-synaptic functions contribute to the impairment of transmission in area CA1 of the Piccolo antisense group. PPF was induced by stimulating afferent fibers twice at intervals of 40 ms, 80 ms and 200 ms. As shown in Fig. 4, there was no difference for all the intervals tested in the PPF among the vehicle-, sense- and antisense-treated groups (ANOVA with repeated measures: group, $F_{(2,29)} = 0.2501$: $p > 0.05$; interval, $F_{(2,58)} = 6.465$, $p < 0.005$; group × interval, $F_{(2,58)} = 0.883$, $p > 0.05$). This result suggests that changes in presynaptic function or the basic properties of synaptic transmission are not involved in the impairment of LTP formation in the Piccolo antisense group.

3.5. Effect of Piccolo antisense injection on glutamate release

In order to clarify whether the impairment of LTP formation in the Piccolo antisense group is attributable to alterations in glutamate release, we measured high K^+-induced glutamate release in the sense- and antisense-treated groups. Although there was no difference in basal glutamate release between the sense- and antisense-treated groups (Fig. 5A), high K^+-induced glutamate release in the Piccolo antisense group was significantly lower than that in sense-treated group (Fig. 5A and B).

4. Discussion

Protein components of the cytoskeletal matrix associated with the CAZ and some scaffolding proteins are involved in endo- and exo-cytosis of synaptic vesicles (Fujimoto et al., 2002; Shibasaki et al., 2004; Fenster et al., 2003). Piccolo is assembled ultrastructurally to form an electron-dense region of the filaments of the CAZ. Recently, it has been reported that the locus and expression level of Piccolo gene, *PCLO*, is involved in a developmental disorder, such as autism and Williams Syndrome, and schizophrenia, which cause emotional and cognitive dysfunction (Fenster and Garner, 2002). In the present study, we administered Piccolo sense and antisense oligonucleotides to mice to investigate the involvement of Piccolo in learning and memory as assessed by behavioral studies and in hippocampal LTP in two different subregions of the hippocampus, area CA1 and the DG.

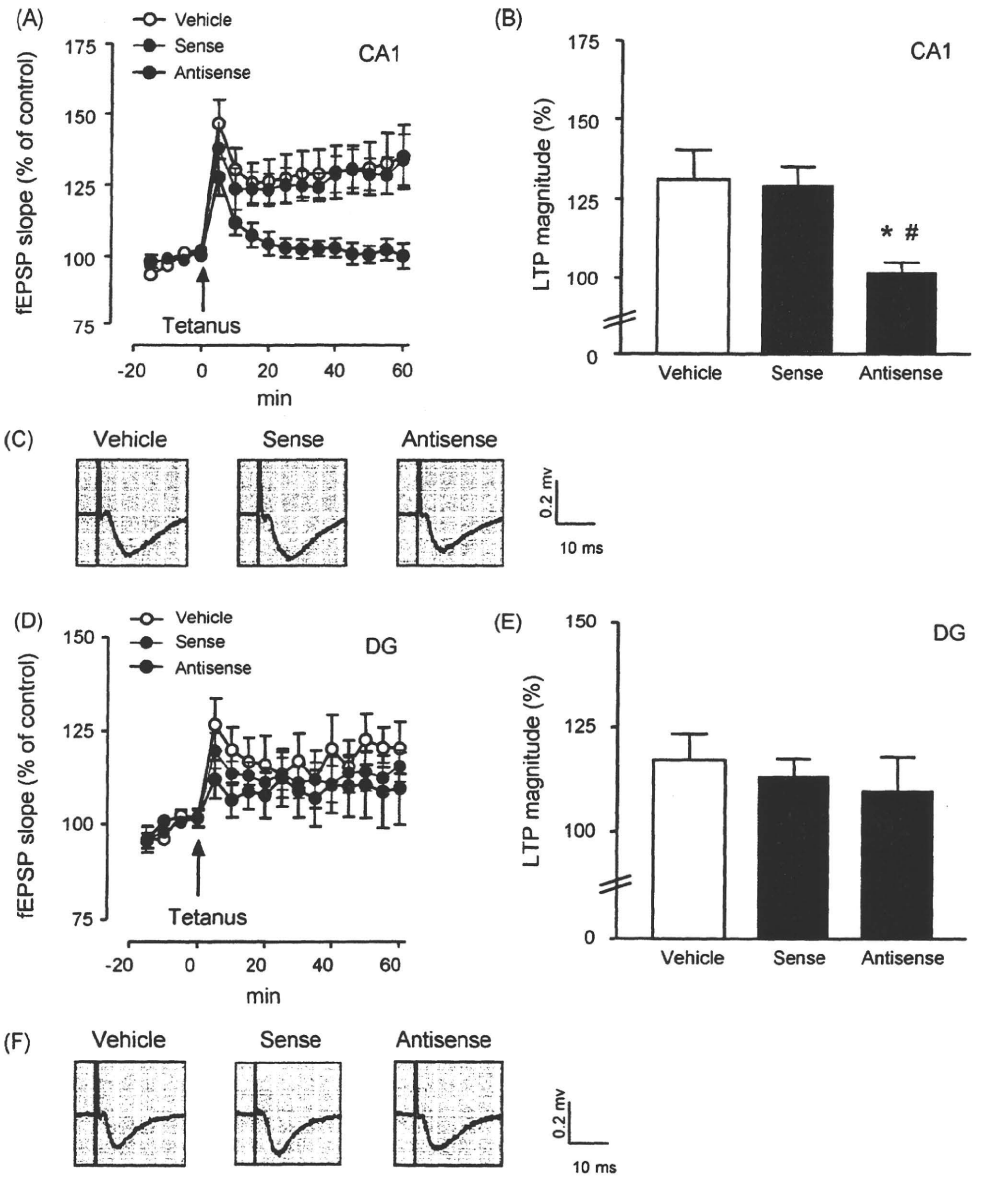

Fig. 3. Effect of Piccolo antisense injection on LTP in area CA1 and the DG in the hippocampus. (A and D) A single 100 Hz tetanic stimulus at $t = 0$ induced LTP in hippocampal slices from Piccolo antisense-, sense- and vehicle-treated mice. Each point represents the mean ± SEM normalized to the EPSP, which was the mean of the EPSP over −15 min to 0 min. (B and E). Comparison of the magnitudes of LTP among antisense-, sense- and vehicle-treated mice. Each column shows the mean ± SEM of the fEPSP expressed as a percentage of the value during 30–60 min after tetanus. Sample recordings of evoked field potentials recorded from the (C) CA1 and (F) DG. The three traces indicate data recorded in the control condition immediately before (white) and 60 min after (black) the tetanic stimulation. Each value represents the mean ± SEM for 6 to 10 experiments. $^*p < 0.05$ vs. vehicle-treated mice. $\#p < 0.05$ vs. sense-treated mice.

Western blot analysis showed that Piccolo protein level was reduced in the hippocampus (Fig. 1A) but not in the cerebral cortex (Fig. 1B) after infusions of Piccolo antisense oligonucleotide. Although the mechanism of the differential sensitivity to antisense in the cerebral cortex and hippocampus is not known, one possible explanation for the regional difference of the effect is that the amount of injected antisense was enough to down-express the Piccolo level in the hippocampus but not in the cerebral cortex. Correspondingly, there was no difference among vehicle-, sense- and antisense-injected mice in the novel object recognition test, which depends more on the cerebral cortex (especially the temporal cortex) than on the hippocampus. In contrast, infusions of antisense oligonucleotide impaired spatial learning as measured by the Morris water maze test. Significantly longer escape latency was observed in the antisense-treated group compared with the vehicle- and sense-treated groups without affecting performance in the visible platform test. Probe test also showed that vehicle- and sense-injected animals spent significantly longer time in the target quadrant than in opposite quadrants; however, such a difference between times spent in two quadrants was not observed in antisense-injected mice. These results indicate that Piccolo plays an important role at least in spatial learning, which depends on the hippocampal function.

LTP in the hippocampus is thought to be a cellular model of learning and memory formation. In this study, measurement of LTP in area CA1 and the DG was carried out simultaneously in a hippocampal slice mounted on a MED system. Down-regulation of the hippocampal Piccolo level by the antisense treatment significantly attenuated LTP in area CA1, whereas infusion of vehicle or Piccolo sense did not affect the LTP (Fig. 3). LTP in the

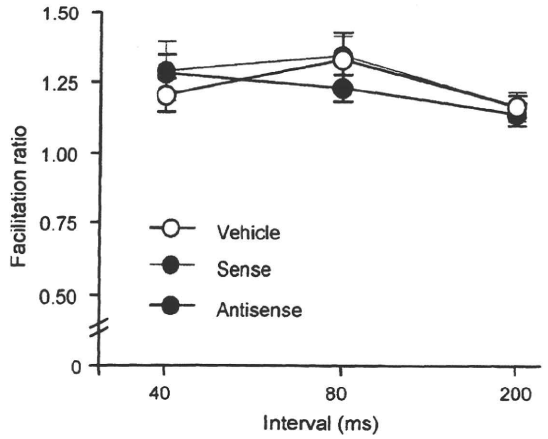

Fig. 4. Effect of Piccolo antisense injection on PPF in area CA1. Comparison of PPF in area CA1 of Piccolo antisense-, sense- and vehicle-treated mice. Facilitation ratio: values represent the facilitation of the second EPSP (S2) relative to the first EPSP (S1). Each value represents the mean ± SEM for 9–13 experiments.

lateral perforant pathway of the DG in the mice injected with Piccolo antisense also tended to be inhibited, but the effect was not significantly compared with the vehicle- or sense-treated mice. The basis of this subregional difference in LTP sensitivity to antisense in hippocampal slices still remains to be elucidated. Earlier reports have shown many functional differences between the Schaffer collateral pathway in area CA1 and the lateral perforant pathway of the DG. Inhibitory neurons, neuronal stem cells and opioid receptors can be observed in relatively large numbers in the lateral perforant pathway of the DG, but are less abundant in the Schaffer collateral pathway of area CA1 (Simmons and Chavkin, 1996; Tozuka et al., 2005; Ito et al., 2001). These differences may cause the different sensitivity to Piccolo antisense in these regions. Nevertheless, our results suggest that attenuated LTP in area CA1 plays, at least in part, a pivotal role in the impairment of spatial learning in mice injected with Piccolo antisense.

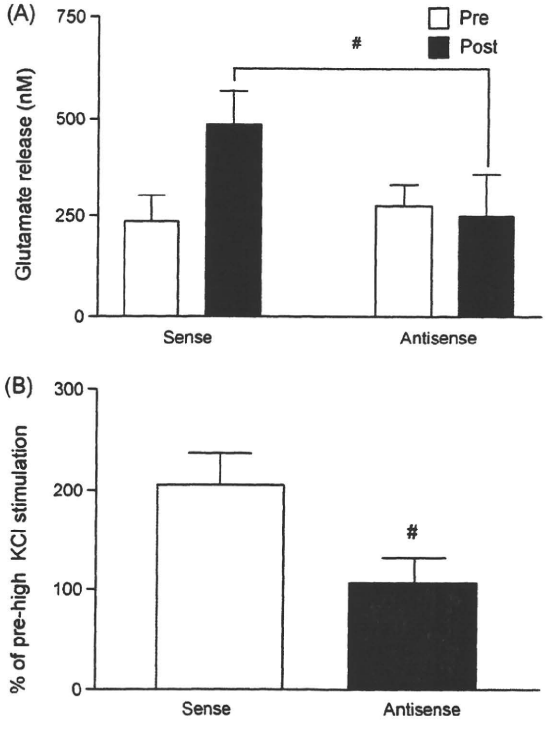

Fig. 5. Effect of Piccolo antisense injection on glutamate release. (A) Glutamate release (nM) and (B) ratio of the control S2 (post-stimulating phase)/S1 (pre-stimulating phase) (%). Each value represents the mean ± SEM for 5–6 experiments. (A and B) #$p < 0.05$ vs. sense-treated mice (two-tailed t-test).

A study of glutamate release from hippocampal slices clearly demonstrated that high K^+-induced glutamate release in antisense-injected mice was significantly lower than in sense-injected mice. These results suggest that the alteration of LTP in antisense-injected mice is attributable, at least in part, to decreased glutamate release from synaptic terminals and/or decreased level of glutamate in the synaptic creft in the hippocampus. In contrast, PPF in area CA1 was not affected by injection of Piccolo antisense. Several studies have demonstrated that PPF increases synaptically activated glial transporter currents in area CA1; however, induction of LTP has no effect on the currents (Levenson et al., 2002; Luscher et al., 1998; Diamond et al., 1998). It is thought that 50 mM KCl has the ability to release glutamate from both neurons and glial cells. Therefore, whether change of glutamate release in antisense-treated mice is caused by depolarization in neuron or not should be clarified further. Since induction and expression of LTP in area CA1 have been shown to require the coordinated regulation of several cellular insults, Piccolo may play a role not only in glutamate release from synaptic terminals but also in other synaptic events such as neuronal glutamate uptake that has been shown to be important for maintaining the level of synaptic strength during LTP (Levenson et al., 2002).

It has also been shown that Bassoon is not essential for synapse formation but plays an essential role in the regulated neurotransmitter release from a subset of glutamatergic synapses (Altrock et al., 2003). The abundance of the other CAZ components in mutant mice lacking the central region of Bassoon revealed that Piccolo levels but not RIM and Munc13 levels are upregulated in $Bsn^{-/-}$ mutants (Altrock et al., 2003). These results suggest that there is functional interaction between Piccolo and Bassoon in synapses. The molecular function of assembly and function of these two proteins in active zone should also be elucidated.

In conclusion, we demonstrated that down-regulation of the level of Piccolo in the hippocampus leads to impairment of spatial learning with a concomitant decrease in LTP in the hippocampus, especially in area CA1. Piccolo may play a role in the regulation of synaptic plasticity by modulating the extracellular glutamate level.

Acknowledgements

This study was supported by a Nihon University Multidisciplinary Global Research Grant and in part by a Grant-in-aid for "Academic Frontier" Project for Private Universities (2007–2011) from the Ministry of Education, Culture, Sports, Science and Technology of Japan, from Uehara Memorial Foundation, International Research Project supported by The Meijo Asian Research Center (MARC), Comprehensive Research on Aging and Health from the Ministry of Health, Labor and Welfare of Japan; by the Mochida Memorial Foundation for Medical and Pharmaceutical Research; and by Japan Canada Joint Health Research Program.

References

Akaishi, T., Nakazawa, K., Sato, K., Ohno, Y., Ito, Y., 2004. 4-Hydroxynonenal modulates the long-term potentiation induced by L-type Ca^{2+} channel activation in the rat dentate gyrus in vitro. Neurosci. Lett. 370, 155–159.

Altrock, W.D., tom, D.S., Sokolov, M., Meyer, A.C., Sigler, A., Brakebusch, C., Fassler, R., Richter, K., Boeckers, T.M., Potschka, H., Brandt, C., Loscher, W., Grimberg, D., Dresbach, T., Hempelmann, A., Hassan, H., Balschun, D., Frey, J.U., Brandstatter, J.H., Garner, C.C., Rosenmund, C., Gundelfinger, E.D., 2003. Functional inactivation of a fraction of excitatory synapses in mice deficient for the active zone protein bassoon. Neuron 37, 787–800.

Cen, X., Nitta, A., Ibi, D., Zhao, Y., Niwa, M., Taguchi, K., Hamada, M., Ito, Y., Ito, Y., Wang, L., Nabeshima, T., 2008. Identification of Piccolo as a regulator of behavioral plasticity and dopamine transporter internalization. Mol. Psychiatry 451–463.

Diamond, J.S., Bergles, D.E., Jahr, C.E., 1998. Glutamate release monitored with astrocyte transporter currents during LTP. Neuron 21, 425–433.

Dick, O., Hack, I., Altrock, W.D., Garner, C.C., Gundelfinger, E.D., Brandstatter, J.H., 2001. Localization of the presynaptic cytomatrix protein Piccolo at ribbon and conventional synapses in the rat retina: comparison with Bassoon. J. Comp. Neurol. 439, 224–234.

Fenster, S.D., Chung, W.J., Zhai, R., Cases-Langhoff, C., Voss, B., Garner, A.M., Kaempf, U., Kindler, S., Gundelfinger, E.D., Garner, C.C., 2000. Piccolo, a presynaptic zinc finger protein structurally related to bassoon. Neuron 25, 203–214.

Fenster, S.D., Garner, C.C., 2002. Gene structure and genetic localization of the PCLO gene encoding the presynaptic active zone protein Piccolo. Int. J. Dev. Neurosci. 20, 161–171.

Fenster, S.D., Kessels, M.M., Qualmann, B., Chung, W.J., Nash, J., Gundelfinger, E.D., Garner, C.C., 2003. Interactions between Piccolo and the actin/dynamin-binding protein Abp1 link vesicle endocytosis to presynaptic active zones. J. Biol. Chem. 278, 20268–20277.

Fujimoto, K., Shibasaki, T., Yokoi, N., Kashima, Y., Matsumoto, M., Sasaki, T., Tajima, N., Iwanaga, T., Seino, S., 2002. Piccolo, a Ca^{2+} sensor in pancreatic beta-cells. Involvement of cAMP-GEFII. Rim2. Piccolo complex in cAMP-dependent exocytosis. J. Biol. Chem. 277, 50497–50502.

Fujimoto, S., Katsuki, H., Kume, T., Kaneko, S., Akaike, A., 2004. Mechanisms of oxygen glucose deprivation-induced glutamate release from cerebrocortical slice cultures. Neurosci. Res. 50, 179–187.

Hammond, R.S., Tull, L.E., Stackman, R.W., 2004. On the delay-dependent involvement of the hippocampus in object recognition memory. Neurobiol. Learn. Mem. 82, 26–34.

Hou, Q., Gao, X., Zhang, X., Kong, L., Wang, X., Bian, W., Tu, Y., Jin, M., Zhao, G., Li, B., Jing, N., Yu, L., 2004. SNAP-25 in hippocampal CA1 region is involved in memory consolidation. Eur. J. Neurosci. 20, 1593–1603.

Ito, Y., Tabata, K., Makimura, M., Fukuda, H., 2001. Acute and chronic intracerebroventricular morphine infusions affect long-term potentiation differently in the lateral perforant path. Pharmacol. Biochem. Behav. 70, 353–358.

Kamei, H., Nagai, T., Nakano, H., Togan, Y., Takayanagi, M., Takahashi, K., Kobayashi, K., Yoshida, S., Maeda, K., Takuma, K., Nabeshima, T., Yamada, K., 2005. Repeated methamphetamine treatment impairs recognition memory through a failure of novelty-induced ERK1/2 activation in the prefrontal cortex of mice. Biol. Psychiatry 59, 75–84.

Levenson, J., Weeber, E., Selcher, J.C., Kategaya, L.S., Sweatt, J.D., Eskin, A., 2002. Long-term potentiation and contextual fear conditioning increase neuronal glutamate uptake. Nat. Neurosci. 5, 155–161.

Luscher, C., Malenka, R.C., Nicoll, R.A., 1998. Monitoring glutamate release during LTP with glial transporter currents. Neuron 21, 435–441.

Matteoli, M., Coco, S., Schenk, U., Verderio, C., 2004. Vesicle turnover in developing neurons: how to build a presynaptic terminal. Trends Cell Biol. 14, 133–140.

Miyamoto, Y., Chen, L., Sato, M., Sokabe, M., Nabeshima, T., Pawson, T., Sakai, R., Mori, N., 2005. Hippocampal synaptic modulation by the phosphotyrosine adapter protein ShcC/N-Shc via interaction with the NMDA receptor. J. Neurosci. 25, 1826–1835.

Nagai, T., Takuma, K., Dohniwa, M., Ibi, D., Mizoguchi, H., Kamei, H., Nabeshima, T., Yamada, K., 2007. Repeated methamphetamine treatment impairs spatial working memory in rats: reversal by clozapine but not haloperidol. Psychopharmacology 194, 21–32.

Oka, H., Shimono, K., Ogawa, R., Sugihara, H., Taketani, M., 1999. A new planar multielectrode array for extracellular recording: application to hippocampal acute slice. J. Neurosci. Methods 93, 61–67.

Powell, C.M., Schoch, S., Monteggia, L., Barrot, M., Matos, M.F., Feldmann, N., Sudhof, T.C., Nestler, E.J., 2004. The presynaptic active zone protein RIM1alpha is critical for normal learning and memory. Neuron 42, 143–153.

Sakata, Y., Chida, R., Ishige, K., Edagawa, Y., Tadano, T., Ito, Y., 2005. Effect of a nutritive-tonic drink on scopolamine-induced memory impairment in mice. Biol. Pharm. Bull. 28, 1886–1891.

Schoch, S., Gundelfinger, E., 2006. Molecular organization of the presynaptic active zone. Cell Tissue Res. 326, 379–391.

Shibasaki, T., Sunaga, Y., Fujimoto, K., Kashima, Y., Seino, S., 2004. Interaction of ATP sensor, cAMP sensor, Ca^{2+} sensor, and voltage-dependent Ca^{2+} channel in insulin granule exocytosis. J. Biol. Chem. 279, 7956–7961.

Simmons, M.L., Chavkin, C., 1996. Endogenous opioid regulation of hippocampal function. Int. Rev. Neurobiol. 39, 145–196.

Tozuka, Y., Fukuda, S., Namba, T., Seki, T., Hisatsune, T., 2005. GABAergic excitation promotes neuronal differentiation in adult hippocampal progenitor cells. Neuron 47, 803–815.

Wang, Y., Okamoto, M., Schmitz, F., Hofmann, K., Sudhof, T.C., 1997. Rim is a putative Rab3 effector in regulating synaptic-vesicle fusion. Nature 388, 593–598.

Weidenhofer, J., Bowden, N.A., Scott, R.J., Tooney, P.A., 2005. Altered gene expression in the amygdala in schizophrenia: up-regulation of genes located in the cytomatrix active zone. Mol. Cell Neurosci. 31, 243–250.

Yamamoto, M., Koshimura, K., Kawaguchi, M., Sohmiya, M., Murakami, Y., Kato, Y., 2000. Stimulating effect of erythropoietin on the release of dopamine and acetylcholine from the rat brain slice. Neurosci. Lett. 292, 131–133.

5702 • The Journal of Neuroscience, April 21, 2010 • 30(16):5702–5712

Neurobiology of Disease

Disrupted Transforming Growth Factor-β Signaling in Spinal and Bulbar Muscular Atrophy

Masahisa Katsuno,[1,2] Hiroaki Adachi,[1] Makoto Minamiyama,[1] Masahiro Waza,[1] Hideki Doi,[1] Naohide Kondo,[1] Hiroyuki Mizoguchi,[3] Atsumi Nitta,[4,5] Kiyofumi Yamada,[5] Haruhiko Banno,[1] Keisuke Suzuki,[1] Fumiaki Tanaka,[1] and Gen Sobue[1]

[1]Department of Neurology, Nagoya University Graduate School of Medicine, Nagoya 466-8550, Japan, [2]Institute for Advanced Research, Nagoya University, Nagoya 464-8601, Japan, [3]Futuristic Environmental Simulation Center, Research Institute of Environmental Medicine, Nagoya University, Nagoya 464-8601, Japan, [4]Department of Pharmaceutical Therapy and Neuropharmacology, Faculty of Pharmaceutical Sciences, Graduate School of Medicine and Pharmaceutical Sciences, University of Toyama, Toyama 930-0194, Japan, and [5]Department of Neuropsychopharmacology and Hospital Pharmacy, Nagoya University Graduate School of Medicine, Nagoya 466-8550, Japan

Spinal and bulbar muscular atrophy (SBMA) is a late-onset lower motor neuron disease caused by the expansion of a trinucleotide CAG repeat, which encodes a polyglutamine tract in androgen receptor (AR). Although it is commonly held that the pathogenic polyglutamine proteins accumulate in neurons and thereby induce transcriptional dysregulation, the downstream molecular events have remained elusive. Here, we examined whether TGF-β signaling is dysregulated in SBMA. Nuclear translocation of phosphorylated Smad2/3, a key step in TGF-β signaling, is suppressed in the spinal motor neurons of male transgenic mice carrying the mutant human *AR*. A similar finding was also observed in the motor neurons, but not in Purkinje cells, of SBMA patients. The pathogenic AR, the causative protein of SBMA, inhibits the transcription of TGF-β receptor type II (TβRII) via abnormal interactions with NF-Y and p300/CBP-associated factor. Furthermore, overexpression of TβRII dampens polyglutamine-induced cytotoxicity in a neuroblastoma cell line expressing the pathogenic AR. The present study thus indicates that disruption of TGF-β due to the transcriptional dysregulation of TβRII is associated with polyglutamine-induced motor neuron damage in SBMA.

Introduction

Polyglutamine disease is a group of hereditary neurodegenerative disorders resulting from the expansion of a genomic trinucleotide CAG repeat, which encodes a polyglutamine tract in causative proteins (Gatchel and Zoghbi, 2005). To date, nine polyglutamine diseases are known: Huntington's disease (HD), spinal and bulbar muscular atrophy (SBMA), dentatorubral-pallidoluysian atrophy, and six forms of spinocerebellar ataxia (SCA1, 2, 3, 6, 7, and 17). SBMA is a lower motor neuron disease caused by an abnormal expansion of a CAG repeat within the androgen receptor (AR) gene (La Spada et al., 1991). Although the causative genes are unrelated except for the expanded CAG repeats, polyglutamine diseases share a common molecular pathogenesis. The expanded polyglutamine tracts alter the conformations of the causative gene products, which then have a strong propensity to accumulate within neurons. It is now commonly held that the accumulation of causative proteins is a pivotal molecular event that triggers the pathogenesis of polyglutamine-mediated neurodegeneration.

Although the molecular mechanism of polyglutamine-induced neuron damage has not been completely elucidated, there is increasing evidence that the accumulation of pathogenic polyglutamine proteins leads to transcriptional dysregulation. This hypothesis has been forwarded by the observation that the polyglutamine aggregates sequester a wide range of transcription factors and coactivators, such as Sp1 and cAMP response element-binding protein-binding protein (CBP) (Nucifora et al., 2001; Dunah et al., 2002). The pathogenic polyglutamine proteins suppress a histone acetyltransferase (HAT) activity of these nuclear proteins, resulting in histone hypoacetylation and eventual downregulation of various gene expressions (Palhan et al., 2005; Sadri-Vakili et al., 2007). In support of this view, pharmacological augmentation of histone acetylation by histone deacetylase (HDAC) inhibitors mitigates the neurodegeneration in cellular and animal models of polyglutamine diseases (Butler and Bates, 2006). Even though it remains unclear which genes are responsible for the pathogenesis of polyglutamine-mediated neurodegeneration, a cDNA microarray study of cultured cells identified a set of genes whose expressions are specifically regulated by HDAC inhibitors (Peart et al., 2005). These genes are

Received Jan. 23, 2010; revised March 8, 2010; accepted March 17, 2010.

This study was supported entirely by grants from the Ministry of Education, Culture, Sports, Science, and Technology, Japan, grants from the Ministry of Health, Labor and Welfare, Japan, and the Program for Improvement of Research Environment for Young Researchers from Special Coordination Funds for Promoting Science and Technology commissioned by the Ministry of Education, Culture, Sports, Science and Technology of Japan and Japan Science and Technology Agency, Core Research for Evolutional Science and Technology. We thank Dr. Seok Hee Park for kindly providing the pTβRII-219/+36 vector.

There were no funding sources other than those described above, and the investigators had sole discretion over study design, collection, analysis, and interpretation of data, writing of the report, and the decision to submit it for publication.

Correspondence should be addressed to either Dr. Masahisa Katsuno or Dr. Gen Sobue, Department of Neurology, Nagoya University Graduate School of Medicine, 65 Tsurumai-cho, Showa-ku, Nagoya 466-8550, Japan, E-mail: ka2no@med.nagoya-u.ac.jp or sobueg@med.nagoya-u.ac.jp.

DOI:10.1523/JNEUROSCI.0388-10.2010

 0270-6474/10/305702-11$15.00/0

components of Myc, transforming growth factor-β (TGF-β), or cycline/cycline-dependent kinase pathways and are relevant to cell survival and proliferation.

Among these HDAC inhibitor-regulated pathways, TGF-β signaling was demonstrated to play a crucial role in the survival and function of adult neurons (Flanders et al., 1998). TGF-β knock-out mice show prominent neuronal cell death together with reduced synaptic density in various parts of the brain (Brionne et al., 2003). TGF-β signaling regulates axon guidance in *Caenorhabditis elegans* and is required for synaptic growth, neurotransmitter release, and neuron morphogenesis in *Drosophila* (Colavita et al., 1998; Zheng et al., 2006). These observations suggest that an impaired TGF-β signaling leads to neuron damage. In the present study, we examined whether TGF-β signaling was dysregulated in SBMA, a polyglutamine-induced motor neuron disease, and how this signaling was involved in the molecular underpinnings of polyglutamine-mediated neurodegeneration.

Materials and Methods

Generation, maintenance, and treatment of transgenic mice. AR-24Q and AR-97Q mice were generated as described previously (Niwa et al., 1991; Katsuno et al., 2002). We used AR-97Q (line 7-8) male mice because they show progressive muscular atrophy and weakness as well as SBMA-like pathology (Katsuno et al., 2003; Waza et al., 2005). In the experiments where it was required, sodium butyrate (a HDAC inhibitor) was administered at a concentration of 4 g/L in distilled water from 5 weeks of age until the end of the analysis, as described previously (Minamiyama et al., 2004). Castration or sham operations were performed on male AR-97Q mice via the abdominal route under pentobarbital anesthesia (40 mg/kg, i.p.) at the age of 5 weeks as described previously (Katsuno et al., 2002). All animal experiments were performed in accordance with the National Institutes of Health *Guide for the Care and Use of Laboratory Animals* and under the approval of the Nagoya University Animal Experiment Committee (Nagoya, Japan).

Immunohistochemistry and immunofluorescence histochemistry. Mice were deeply anesthetized with pentobarbital and perfused with PBS followed by 4% paraformaldehyde fixative in phosphate buffer, pH 7.4. Whole brains, spinal cords, brainstems, and skeletal muscles were removed and embedded in paraffin. Autopsy specimens of lumbar spinal cord were obtained from genetically diagnosed SBMA patients (52- and 78-year-old males) and from neurologically normal patients (58- and 75-year-old males). The collection of human tissues and their use for this study were approved by the Ethics Committee of Nagoya University Graduate School of Medicine. Six-micrometer-thick sections were prepared from paraffin-embedded tissues, and immunohistochemistry and immunofluorescence were performed as described previously (Katsuno et al., 2006b; Tokui et al., 2009). Sections to be immunostained for TGF-β receptor type II (TβRII) or TGF-β were first microwaved for 20 min in 50 mM citrate buffer, pH 6.0. Sections to be immunostained for polyglutamine (1C2 antibody) were treated with formic acid for 5 min at room temperature. Cells to be immunostained were fixed with 4% paraformaldehyde fixative in phosphate buffer, pH 7.4, and treated with PBS containing 0.1% Triton X-100. All the specimens were treated with TNB blocking buffer (PerkinElmer) before incubation with primary antibodies, and immunoreactivity was detected using EnVision+ System-HRP (DakoCytomation). The immunohistochemical sections were photographed with an optical microscope (BX51, Olympus), and immunofluorescent specimens were photographed with an upright microscope (Axio Imager M1, Zeiss). Fluorescent intensities were measured as described previously (Adachi et al., 2001; Katsuno et al., 2006b). Briefly, fluorescent intensities were measured in >20 neurons within three nonconsecutive sections from each of three AR-97Q mice. For the purposes of counting, a motor neuron was defined by its presence within the anterior horn and the obvious nucleolus in a given 6-μm-thick section. The intensities and cell sizes were quantified with Image Gauge software version 4.22 (Fujifilm). The following primary antibodies were used: anti-pSmad2/3 (3101, Cell Signaling Technology, 1:5000), anti-polyglutamine (1C2) (MAB1574, Millipore, 1:20,000), anti-choline acetyltransferase (AB144, Millipore, 1:1000), anti-pan-specific TGF-β (AB-100-NA, R & D Systems, 1:1000), anti-TβRI (RB-10455, Thermo Scientific, 1:200), anti-TβRII (RB-10345, Thermo Scientific, 1:200), anti-NF-Y (sc-17753, Santa Cruz Biotechnology, 1:500), and anti-p300/CBP-associated factor (P/CAF) (ab12188, Abcam, 1:200). Alexa-conjugated secondary antibodies (Invitrogen) were used for immunofluorescence. Fluorescent Nissl staining was performed using NeuroTrace (Invitrogen, 1:200).

Immunoblotting, immunoprecipitation, and filter trap assay. Mice were killed under pentobarbital anesthesia. Tissues (whole brains, spinal cord, brainstem, and skeletal muscles) were dissected free, snap frozen with powdered CO_2 in acetone, and homogenized in CelLytic lysis buffer (Sigma-Aldrich) containing a phosphatase inhibitor mixture (Sigma-Aldrich) and a protease inhibitor mixture (Thermo Scientific). SH-SY5Y cells were lysed in CelLytic lysis buffer containing a protease inhibitor mixture 36 h after transfection. Nuclear and cytoplasmic fractions were extracted using NE-PER nuclear and cytoplasmic extraction reagents (Thermo Scientific). The homogenates were centrifuged at 2500 × *g* for 15 min at 4°C. The supernatant fractions were separated on 5–20% SDS-PAGE gels and then transferred to Hybond-P membranes (GE Healthcare) using 25 mM Tris, 192 mM glycine, 0.1% SDS, and 10% methanol as transfer buffer. Primary and secondary antibodies were diluted with Can Get Signal, a signal enhancer solution (NKB-101, Toyobo). The immunoblots were digitalized (LAS-3000 imaging system, Fujifilm), signal intensities of three independent blots were quantified with Image Gauge software version 4.22 (Fujifilm), and the means ± SEM were expressed in arbitrary units. The following primary antibodies were used: anti-pSmad2/3 (3101, Cell Signaling Technology, 1:200), anti-Smad2/3 (3102, Cell Signaling Technology, 1:300), anti-pSmad1/5/8 (9511, Cell Signaling Technology, 1:300), anti-histone H1 (05-457, Millipore, 1:300), anti-α-tubulin (T5168, Sigma-Aldrich, 1:5000), anti-pan-specific TGF-β (AB-100-NA, R & D Systems, 1:200), anti-TβRI (RB-10455, Thermo Scientific, 1:200), anti-TβRII (RB-10345, Thermo Scientific, 1:200), anti-V5 (R960-25, Invitrogen, 1:1000), anti-AR (N-20) (sc-816, Santa Cruz Biotechnology, 1:1000), anti-P/CAF (ab12188, Abcam, 1:500), anti-NF-Y (sc-17753, Santa Cruz Biotechnology 1:500), and anti-acetyl histone H3 (06-599, Millipore, 1:500). Primary antibody binding was probed using horseradish peroxidase-conjugated secondary antibodies (GE Healthcare) at a dilution of 1:5000, and bands were detected using the ECL Plus kit (GE Healthcare). Immunoprecipitation was performed as described previously (Adachi et al., 2003). Briefly, AR-containing immune complexes were precipitated using 300 μg of the total protein lysate in radioimmunoprecipitation assay buffer, 30 μl of protein G-Sepharose (GE Healthcare), and 5 μg of antibody anti-P/CAF (sc-13124, Santa Cruz Biotechnology), anti-NF-Y (sc-17753, Santa Cruz Biotechnology) or normal mouse IgG (Thermo Scientific). Proteins were eluted from beads and loaded on SDS-polyacrylamide gels. Blots were sequentially probed with an anti-AR antibody (sc-816, Santa Cruz Biotechnology, 1:1000) and then with anti-rabbit IgG (TrueBlot, eBioscience, 1:1000). Signal intensities of three independent blots were quantified with Image Gauge software version 4.22 (Fujifilm), and percentage input was calculated. Filter trap assay was performed as described previously (Adachi et al., 2003, 2007). Briefly, SH-SY5Y cells were lysed in 50 mM Tris pH 8.0, 150 mM NaCl, 1% Nonidet P-40, 0.5% deoxycholate, 1 mM 2-mercaptoethanol, and 2% SDS, and samples of protein (100 μg) were filtrated through an upper 0.2 μm cellulose acetate membrane (Sartorius) and a lower 0.45 μm nitrocellulose membrane (Bio-Rad) using a Bio-Dot apparatus (Bio-Rad). Blots were probed as described for immunoblots.

Quantitative real-time PCR. TGF-β inducible early gene (TIEG) and TβRII1 mRNA levels were determined by real-time PCR as described previously (Katsuno et al., 2006b). Briefly, total RNA was extracted from mouse spinal cord using TRIzol reagent (Invitrogen) and from cells using the RNeasy Mini kit (Qiagen). The extracted RNA was then reverse transcribed into first-strand cDNA using SuperScript III reverse transcriptase (Invitrogen). Real-time PCR was performed in a total volume of 50 μl containing 25 μl of 2× QuantiTect SYBR Green PCR Master Mix and 0.4 μM each primer (Qiagen), and the amplified products were detected by

the iCycler system (Bio-Rad). The reaction conditions were 95°C for 15 min and then 45 cycles of 15 s at 95°C followed by 60 s at 55°C. For an internal standard control, the expression level of glyceraldehyde-3-phosphate dehydrogenase (GAPDH) was quantified simultaneously. The following primers were used: 5′-aagctgcttccagtcaggat-3′ and 5′-ttgaactcaggtcgtcttgc-3′ for mouse TβRII, 5′-tcaagaaggtggtgaagcag-3′ and 5′-gttgaagtcgcaggagacaa-3′ for mouse GAPDH, 5′-gaagaacccacggaaatgtt-3′ and 5′-tctcatcaccatcggacact-3′ for mouse TIEG, 5′-taccttcatgggttgcagaa-3′ and 5′-aaggctgggagcagagaata-3′ for human TβRII, and 5′-ctcctcctgttcgacagtca-3′ and 5′-caatacgaccaaatccgttg-3′ for human GAPDH. The threshold cycle of each gene was determined as the number of PCR cycles at which the increase in reporter fluorescence was 10 times the baseline signal. The weight of the gene contained in each sample was equal to the log of the starting quantity, and the standardized expression level in each mouse was equal to the weight ratio of each gene to that of GAPDH. PCRs were repeated four times for each of the indicated numbers of samples.

Plasmid, cell culture, and transfection. Human truncated AR cDNAs containing 24 or 97 CAGs (1-645 and 1-864 bp, respectively) were isolated from pCR3.1 full-length AR-24Q or AR-97Q vectors (Waza et al., 2005), and subcloned into pcDNA 6.2/V5-GW/D-TOPO (Invitrogen). The fragments were then subcloned into the pcDNA6.2/c-EmGFP vector (Invitrogen). Human TβRII cDNA was also subcloned into pcDNA6/V5-His (Invitrogen). For the luciferase assay, the pTβRII-219/+36 vector encoding firefly luciferase, kindly provided by Dr. Seok Hee Park (Department of Biological Science, Sungkyunkwan University, Korea), and the pRL-TK vector encoding *Renilla* luciferase (Promega) were transfected into SH-SY5Y cells.

Human neuroblastoma cells (SH-SY5Y, American Type Culture Collection No. CRL-2266) were plated in DMEM/F12 containing 10% fetal bovine serum with penicillin and streptomycin. Each dish was transfected with the indicated vectors using Opti-MEM (Invitrogen) and Lipofectamine 2000 (Invitrogen) and then differentiated in DMEM/F12 supplemented with 2% fetal calf serum, 10 μM retinoic acid, and 2 ng/ml recombinant human TGF-β2 (302-B2, R & D Systems) for 36 h. Sodium butyrate (NaB) dissolved in PBS was added to the differentiation medium at the indicated concentrations. The anti-pan-specific TGF-β antibody (R & D Systems) was applied at a concentration of 5 μg/ml to neutralize TGF-β signaling. The oligonucleotide small interfering RNA (siRNA) duplex against TβRII (Stealth RNAi duplex, HSS 110701) and that against P/CAF (Stealth RNAi duplex, HSS 113059) were synthesized by Invitrogen. SH-SY5Y cells were transfected with either of these siRNAs or with control oligonucleotide (Stealth RNAi negative control duplex, Invitrogen) by using Lipofectamine RNAiMAX (Invitrogen) according to the manufacturer's instructions. Each siRNA was transfected at a concentration of 30 nM.

Luciferase activity and cell viability assay. For the luciferase assay, cell extracts were prepared 36 h after transfection by a detergent lysis method (Promega). Luciferase activity was measured with a luminometer (Lumi-Counter 2500, Microtec) and the Dual-Luciferase reporter assay system (Promega). The ratio of firefly luciferase activity to *Renilla* luciferase activity in each sample served as a measure of the relative luciferase activity. Each construct was transfected at least three times, and data for each construct are presented as means ± SEM.

Cell death analysis was performed as described previously (Katsuno et al., 2006b). Briefly, 36 h after transfection, cells were stained with propidium iodide (Invitrogen) and mounted with VECTASHIELD mounting medium (Vector Laboratories). Quantitative analyses were made from triplicate determinations. Duplicate slides were graded blindly in two independent trials as described previously (Katsuno et al., 2005). The cell viability assay was performed using WST-1 (Roche Diagnostics) according to the manufacturer's instructions. Briefly, cells were cultured in 24-well plates. After treatments, cells were incubated with WST-1 substrate for 2–3 h and spectrophotometrically assayed at 440 nm using a plate reader (Powerscan HT, Dainippon Pharmaceutical).

Statistical analyses. Data were analyzed using the Kaplan–Meier and log-rank tests for survival rate, ANOVA with a *post hoc* test (Dunnett or Turkey–Kramer) for multiple comparisons, two-way ANOVA with repeated measures for mouse behavior analysis, Pearson's coefficient for correlation, and an unpaired *t test* from StatView software, version 5 (Hulinks).

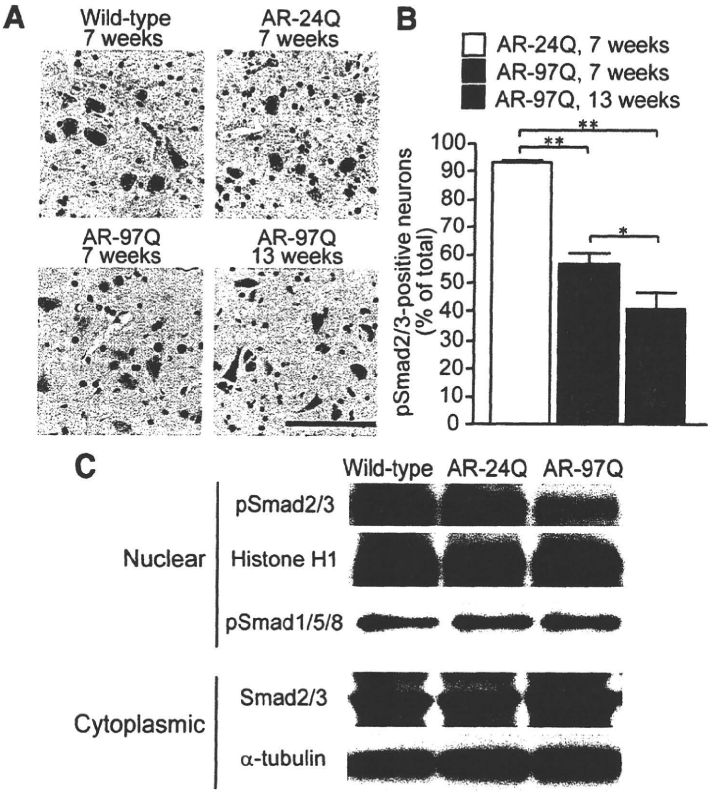

Figure 1. Nuclear translocation of Smad2/3 in SBMA mice. ***A***, Anti-phosphorylated Smad2/3 (pSmad2/3) immunohistochemistry of the spinal cords from wild-type, AR-24Q, and AR-97Q mice. Scale bar, 100 μm. ***B***, The frequency of pSmad2/3 staining in spinal motor neurons of AR-24Q and AR-97Q mice. Error bars indicate SEM; $*p < 0.05$, $**p < 0.01$. ***C***, Immunoblots of the nuclear and cytoplasmic fractions from the spinal cords of wild-type, AR-24Q, and AR-97Q mice (7 weeks old).

Results

Pathogenic AR inhibits nuclear translocation of phosphorylated Smad2/3

The biological properties of TGF-β are mediated by a high-affinity transmembrane receptor serine/threonine kinase complex consisting of TβRI and TβRII. Ligand interaction with a homodimer of TβRII recruits and activates TβRI, which in turn phosphorylates the receptor-regulated Smad proteins (Smad2 and 3). Phosphorylated Smad2/3 (pSmad2/3) then translocate into the nucleus, where the molecules regulate target gene transcription (Shi and Massague 2003). To examine whether TGF-β signaling is altered in SBMA, we first investigated the nuclear translocation of Smad2/3 in a transgenic mouse model of SBMA (Katsuno et al., 2002). In immunohistochemistry, pSmad2/3 was intensely stained in the nuclei of almost all neurons and glial cells within the spinal anterior horn of wild-type mice and AR-24Q

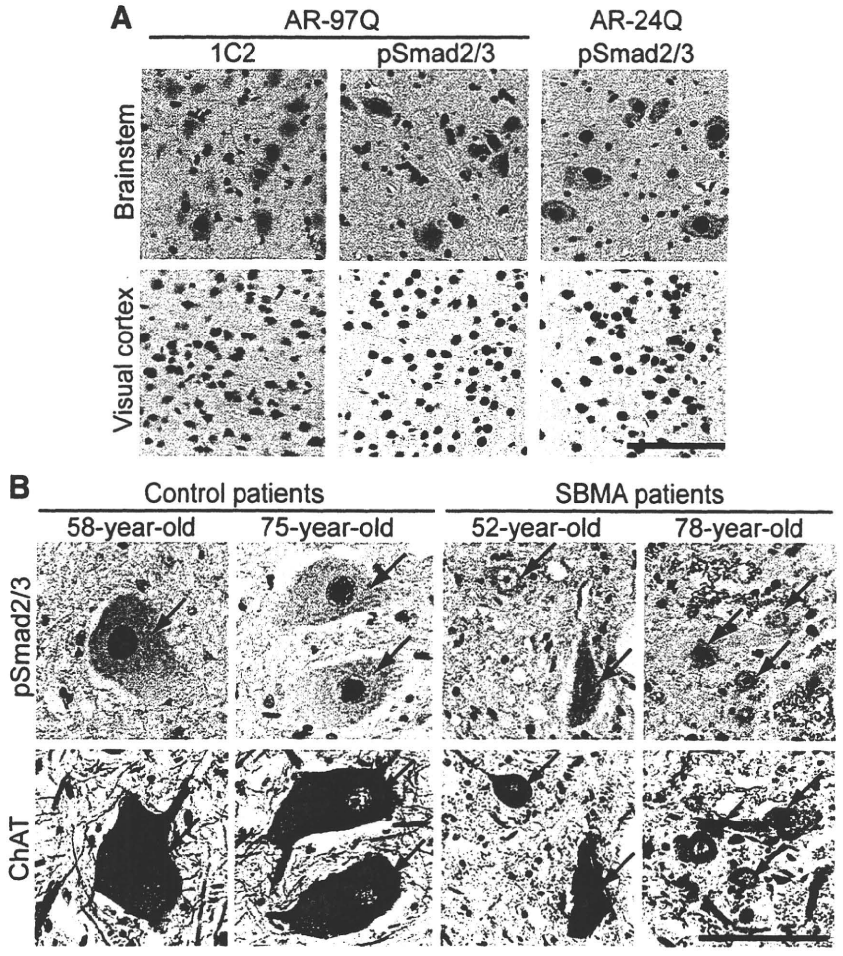

Figure 2. Specificity of Smad2/3 hypophosphorylation in SBMA mice and patients. ***A***, Anti-expanded polyglutamine (1C2) and anti-pSmad2/3 immunohistochemistry of the brainstem and cerebral cortex from AR-24Q, and AR-97Q mice (13 weeks old). Phosphorylation of Smad2/3 is decreased in motor neurons within the motor trigeminal nucleus in the pons, but not in neurons within the visual cortex. ***B***, Anti-pSmad2/3 and anti-choline acetyltransferase (ChAT) immunohistochemistry of serial sections of the spinal cord from control subjects and SBMA patients. Arrows indicate identical neurons in each patient. ChAT-positive motor neurons of the SBMA patient are atrophied and show a decreased immunoreactivity for pSmad2/3 in the nucleus. Scale bars, 100 μm.

transgenic mice bearing normal human *AR* containing 24 CAGs (Fig. 1*A*,*B*). By contrast, immunoreactivity of pSmad2/3 was notably diminished in nuclei of AR-97Q transgenic mice carrying the disease-related mutant *AR* with 97 CAGs (Fig. 1*A*). Although the onset of motor impairment in AR-97Q mice is ~8–10 weeks, decreased pSmad2/3 was evident at 7 weeks, a preonset stage in these mice (Fig. 1*A*,*B*). Immunoblotting confirmed a significant reduction in pSmad2/3 protein from the nuclear fractions of the AR-97Q mouse spinal cords (Fig. 1*C*). Signal intensities of the pSmad2/3-immunoreactive bands normalized to histone H1 were significantly decreased in the spinal cord of AR-97Q mice (AR-24Q, 0.89 ± 0.12; AR-97Q, 0.28 ± 0.05; $p < 0.0005$; 7 weeks old; $n = 3$). This profound decrease in pSmad2/3 signal in immunoblot may result from both neuronal and glial accumulation of pathogenic AR due to a wide expression of the transgene driven by a potent promoter in the mouse model (Katsuno et al., 2002). Despite a significant decrease in nuclear pSmad2/3, AR-97Q mice showed no alterations in phosphorylated Smad1/5/8, the downstream signal molecules regulated by bone morphogenetic protein (BMP) (Fig. 1*C*). To test whether TGF-β signaling is disrupted in the mouse model of SBMA, we measured the levels of TIEG mRNA, the expression of which is controlled by TGF-β. The mRNA levels of TIEG normalized to GAPDH were significantly decreased in the spinal cord of AR-97Q mice (AR-24Q, $3.66 \pm 0.59 \times 10^{-3}$; AR-97Q, $2.22 \pm 0.77 \times 10^{-3}$; $p < 0.01$; 7 weeks old; $n = 4$), suggesting that TGF-β signaling is inhibited in the transgenic mouse model of SBMA.

To confirm that the decreased nuclear translocation of pSmad2/3 is specific to the affected brain regions in SBMA, we compared immunohistochemistry in different areas of the mouse brain. These results showed that nuclear translocation of pSmad2/3 was inhibited in the brainstem, where anti-polyglutamine immunoreactivity is strongly detected, but not in the visual cortex, which is not affected in AR-97Q mice (Fig. 2*A*). As pathogenic AR also accumulates in the nuclei of non-neural tissues in AR-97Q mice (Katsuno et al., 2002), we also examined TGF-β signaling in skeletal muscle. Phosphorylated Smad2/3 was decreased in the nuclei of skeletal muscle cells from AR-97Q mice, suggesting a noncell type-specific disruption of TGF-β signaling (supplemental Fig. 1*A*,*B*). On the contrary, nuclear staining of pSmad2/3 was not diminished in motor neurons within the spinal anterior horn of the mutant superoxide dismutase 1 (SOD1) G93A transgenic mouse, an animal model of amyotrophic lateral sclerosis (ALS), at an early symptomatic stage (supplemental Fig. 2, available at www.jneurosci.org as supplemental material). We further examined whether TGF-β signaling is impaired in patients with SBMA. In autopsied spinal cords from SBMA patients, nuclear immunoreactivity of pSmad2/3 was notably diminished in motor neurons (Fig. 2*B*). By contrast, nuclear staining of pSmad2/3 was not diminished in the patients' glial cells, in which pathogenic AR accumulation has rarely been observed (Li et al., 1998; Adachi et al., 2005). Furthermore, nuclear translocation of pSmad2/3 was not inhibited in the cerebellar Purkinje cells, which are not affected in SBMA, suggesting that the impairment of TGF-β signaling is specific to pathological lesions of this disease (supplemental Fig. 3, available at www.jneurosci.org as supplemental material).

The accumulation of pathogenic AR in the nuclei of motor neurons is the pivotal step leading to neurodegeneration in SBMA. To test the relationship between the nuclear accumulation of pathogenic AR and the reduced activation (i.e., phosphorylation and nuclear translocation) of Smad2/3, we performed immunohistochemistry on the spinal cords of AR-97Q mice using antibodies against expanded polyglutamine (1C2) and pSmad2/3. In the spinal anterior horn, there was significantly less pSmad2/3 immunoreactivity in the motor neurons showing nuclear accumulation of pathogenic AR than in those without 1C2 nuclear staining (Fig. 3*A*). Quantitative analysis showed that the

intensity of pSmad2/3 immunoreactivity in 1C2-positive motor neurons from AR-97Q mice was reduced to 36.1 ± 40.1% of that from 1C2-negative neurons ($p < 0.05$; 8–9 weeks old; $n = 3$ for each group). The pSmad2/3 immunoreactivity was positively correlated with the size of spinal motor neurons ($r = 0.689$, $p < 0.0001$), suggesting a link between TGF-β signal disruption and neuronal dysfunction (Fig. 3*B*). As observed in the mice, there was less pSmad2/3 immunoreactivity in 1C2-positive motor neurons than in those without nuclear accumulation of pathogenic AR in the autopsied spinal cord of an SBMA patients (Fig. 3*C*). These observations suggest that TGF-β signaling is interrupted in the neurons bearing nuclear accumulation of pathogenic AR.

To investigate the cause of TGF-β signal disruption, we first examined the levels of the ligand using an antibody against pan TGF-β isoforms. TGF-β immunoreactivity was not decreased in AR-97Q mouse spinal cord (Fig. 3*D*). This finding was consistent with immunoblotting that demonstrated no reduction in the amount of TGF-β in AR-97Q mice at both preonset and symptomatic stages (Fig. 3*E*).

Expression of TβRII is decreased in SBMA

The diminished nuclear translocation of pSmad2/3 along with an intact level of TGF-β suggests the involvement of TGF-β receptors. It is known that the TGF-β receptors TβRI and TβRII are widely expressed in the CNS, both during development and in adulthood (Vivien and Ali, 2006). Immunoreactivities for both TβRI and TβRII were detected in the spinal motor neurons of wild-type mice (Fig. 4*A*); however, spinal motor neuron staining for TβRII, but not for TβRI, was decreased in AR-97Q mice even before the onset of neuromuscular symptoms (Fig. 4*A*). Immunoblotting confirmed a significant reduction in TβRII protein in the spinal cords of AR-97Q mice (Fig. 4*B*). Signal intensities of the TβRII-immunoreactive bands normalized to α-tubulin were significantly decreased in the spinal cords of AR-97Q mice (AR-24Q, 0.27 ± 0.03; AR-97Q, 0.16 ± 0.04; $p < 0.05$; 7 weeks old; $n = 3$). The mRNA levels of TβRII normalized to GAPDH were significantly decreased in the spinal cords of AR-97Q mice (AR-24Q, 1.38 ± 0.16 × 10^{-2}; AR-97Q, 0.93 ± 0.33 × 10^{-2}; $p < 0.001$; 7 weeks old; $n = 4$), suggesting that the expression of this receptor is suppressed.

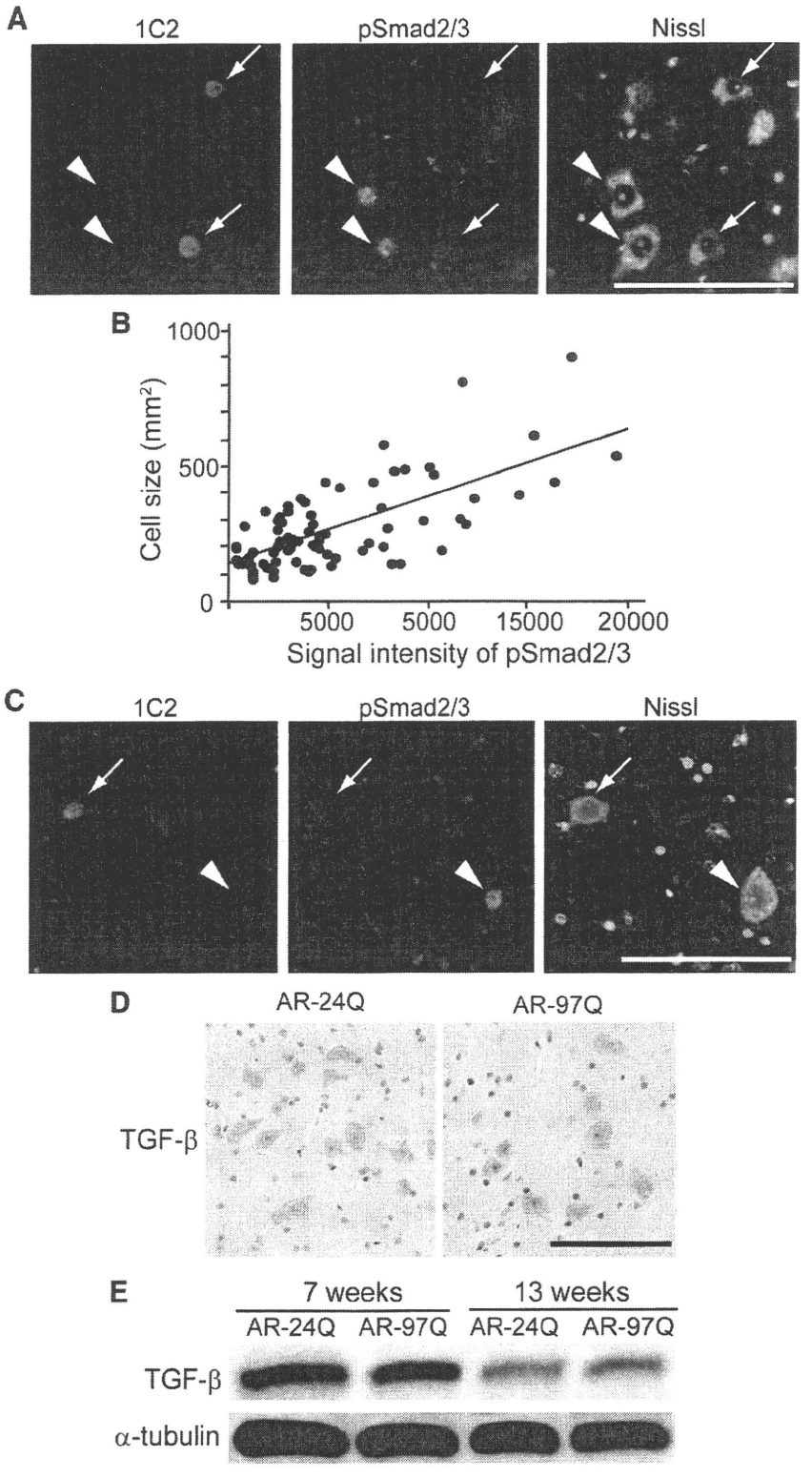

Figure 3. Phosphorylated Smad2/3 and TGF-β expression in SBMA mice. ***A***, Anti-expanded polyglutamine AR (1C2, red) and anti-phosphorylated Smad2/3 (green) double immunofluorescence histochemistry in the spinal cord from an AR-97Q mouse (8 weeks old). Immunoreactivity for pSmad2/3 is detected in 1C2-negative neurons (arrowheads), but not in 1C2-positive cells (arrows). ***B***, Correlation between the intensity of pSmad2/3 immunoreactivity and the size of motor neurons in the spinal cord of AR-97Q mice (8–9 weeks old, $n = 4$). ***C***, 1C2 and anti-phosphorylated Smad2/3 double immunofluorescence histochemistry in the spinal cord of an SBMA patient. ***D***, Immunohistochemistry in the spinal cords from AR-24Q and AR-97Q mice using a pan-specific antibody against TGF-β isoforms (13 weeks old). ***E***, Immunoblots of the spinal cords of AR-24Q and AR-97Q mice. Scale bars, 100 μm.

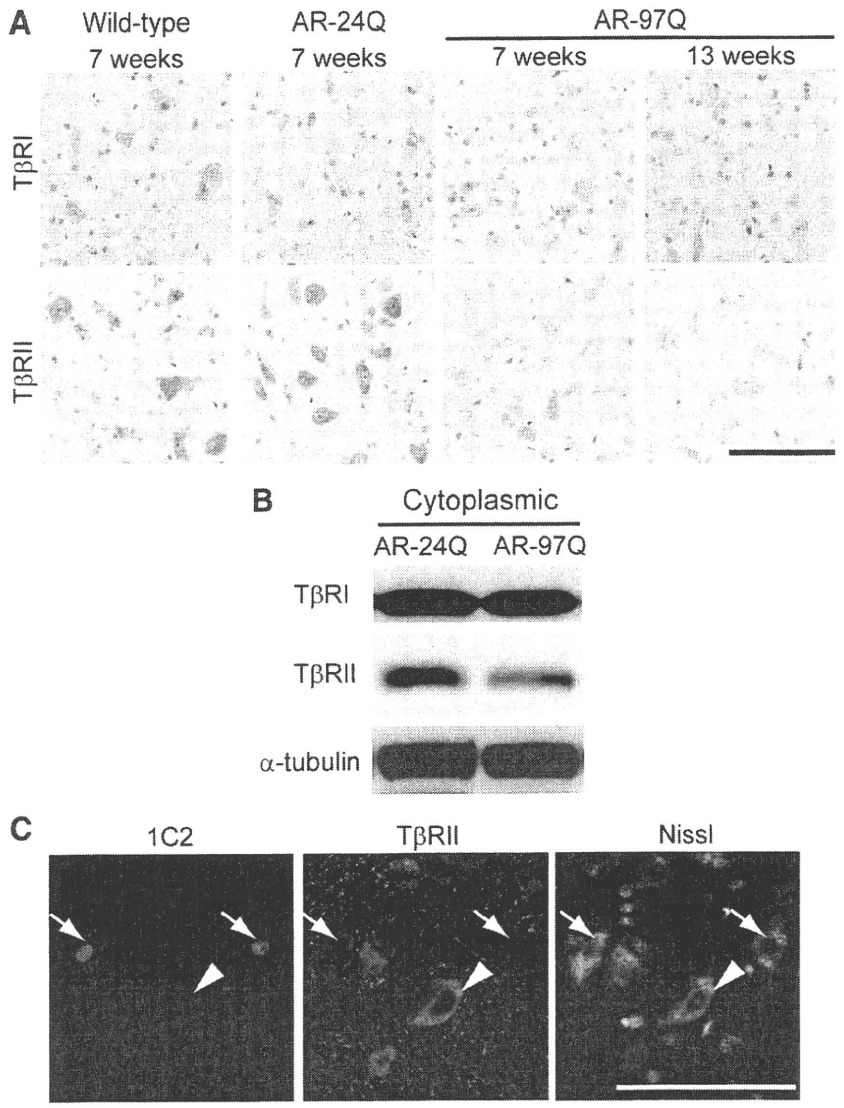

Figure 4. Expression of TGF-β receptors in SBMA mice. ***A***, Immunohistochemistry in the spinal cords from wild-type, AR-24Q, and AR-97Q mice using antibodies against the TGF-β receptors TβRI and TβRII. ***B***, Immunoblots of the cytoplasmic fractions of the spinal cords from AR-24Q and AR-97Q mice (7 weeks old). ***C***, 1C2 and anti-TβRII double immunofluorescence histochemistry in the spinal cord from an AR-97Q mouse (8 weeks old). Immunoreactivity for TβRII is detected in 1C2-negative neurons (arrowheads), but not in 1C2-positive cells (arrows). Scale bars, 100 μm.

To confirm that the decreased TβRII expression is specific to affected neurons, we performed double immunofluorescence histochemistry using 1C2 together with an antibody against TβRII (Fig. 4*C*). Quantitative analysis showed that the intensity of TβRII immunoreactivity in 1C2-positive motor neurons was reduced to 25.8 ± 37.1% of that from 1C2-negative neurons ($p < 0.0001$; 8–9 weeks old; $n = 3$ for each group). Reduced TβRII immunoreactivity was also detected in an autopsied spinal cord from an SBMA patient (Fig. 5*A*). Furthermore, TβRII immunofluorescence in this SBMA patient was more reduced in 1C2-positive motor neurons than in those without nuclear accumulation of the pathogenic AR (Fig. 5*B*).

SBMA only affects males, whereas females carrying the AR mutation scarcely show symptoms (Katsuno et al., 2006a). Previous studies showed that the pathogenic AR containing an expanded polyglutamine tract accumulates in the nuclei of motor neurons in a testosterone-dependent manner, and that inhibition of testosterone production prevents this accumulation (Katsuno et al., 2002; Takeyama et al., 2002). Furthermore, testosterone reduction, by castration or medication, mitigates neurodegeneration in SBMA mice and patients (Katsuno et al., 2003; Chevalier-Larsen et al., 2004; Banno et al., 2009). We thus examined whether castration restores the TGF-β-Smad2/3 signal pathway in male AR-97Q mice. Both immunohistochemistry and immunoblotting demonstrated that castration increased the expression of TβRII and restored the nuclear translocation of pSmad2/3 (supplemental Fig. 4*A*,*B*). Together, these findings suggest that the accumulation of the pathogenic AR proteins interferes with TGF-β signaling through downregulation of TβRII expression in SBMA mice and patients.

Pathogenic AR dysregulates transcription of TβRII

To clarify the molecular mechanism by which pathogenic AR suppresses the expression of TβRII, we studied its transcriptional regulation in a cultured cell model of SBMA, SH-SY5Y cells harboring an N-terminal fragment of human AR containing an expanded polyglutamine tract and a part of AF-1 domain [truncated AR-97Q (tAR97Q)]. Phosphorylated Smad2/3 was significantly lower in the nuclear fraction of these cells than in cells bearing tAR24Q (Fig. 6*A*,*B*; supplemental Fig. 5, available at www.jneurosci.org as supplemental material), and TβRII protein was reduced in the cytoplasmic fraction of cells carrying tAR97Q (Fig. 6*A*,*C*). Quantitative RT-PCR analysis showed that TβRII mRNA normalized to GAPDH was also significantly diminished in tAR97Q-transfected cells compared with those transfected with tAR24Q (tAR24Q, $1.80 \pm 0.17 \times 10^{-4}$; tAR97Q, $1.11 \pm 0.02 \times 10^{-4}$; $p < 0.0005$; $n = 4$ per group). To test whether pathogenic AR suppresses the expression of TβRII at the transcriptional level, we investigated TβRII promoter activity using a luciferase reporter assay. The activity of luciferase, controlled by the TβRII promoter, was significantly decreased in a dose-dependent manner in tAR97Q-transfected cells compared with those transfected with tAR24Q (Fig. 6*D*), suggesting that the pathogenic AR protein bearing an expanded polyglutamine tract downregulates the transcription of TβRII.

Recent reports indicated that the transcription of TβRII is regulated by the transcription factor NF-Y, which binds to the inverted CCAAT box within the promoter region of TβRII, and by P/CAF, a transcriptional coactivator with HAT activity (Park et al., 2002). Therefore, we next examined whether pathogenic AR interferes with NF-Y and P/CAF in cultured cells. Immunocytochemical analysis demonstrated that green fluorescent protein (GFP)-tagged pathogenic AR was confined to inclusion bodies, to which NF-Y or P/CAF were colocalized (Fig. 7*A*,*B*).

The AR proteins, tAR24Q and tAR97Q, were coimmunoprecipitated with P/CAF or NF-Y (Fig. 7*C*). Quantitative analyses showed that the pathogenic AR preferably binds to P/CAF, although this was not the case for NF-Y (Fig. 7*D*).

To confirm the interaction between the pathogenic AR aggregates and the nuclear proteins P/CAF and NF-Y, we performed filter trap assay. In this analysis, the larger-sized protein complex was retained on the cellulose acetate membrane (pore diameter, 0.2 μm), whereas the nitrocellulose membrane captured proteins of all sizes (Adachi et al., 2003). The results showed that both P/CAF and NF-Y were retained on a cellulose acetate membrane together with tAR97Q, but not with tAR24Q, suggesting that these nuclear proteins were confined in a large molecular weight complex of tAR97Q (Fig. 7*E*). Additionally, the amounts of NF-Y and P/CAF in soluble fraction were decreased (Fig. 7*F*).

We showed previously that oral administration of NaB, a potent HDAC inhibitor, facilitates histone acetylation and thereby improves motor functions of AR-97Q mice (Minamiyama et al., 2004). Because the induction of histone acetylation was shown to upregulate the TβRII promoter activity (Park et al., 2002), we further tested whether NaB restores TGF-β signaling. In the SH-SY5Y cells expressing tAR97Q, NaB increased the amounts of TβRII and pSmad2/3 (supplemental Fig. 6*A*, available at www.jneurosci.org as supplemental material). These effects were suppressed by knock-down of P/CAF, suggesting that NaB-mediated facilitation of TGF-β signaling at least partially depends on P/CAF activity (supplemental Fig. 6*A*, available at www.jneurosci.org as supplemental material). Moreover, the expressions of TβRII and nuclear pSmad2/3 were higher in AR-97Q mice treated with NaB than in untreated mice (supplemental Fig. 6*B*,*C*).

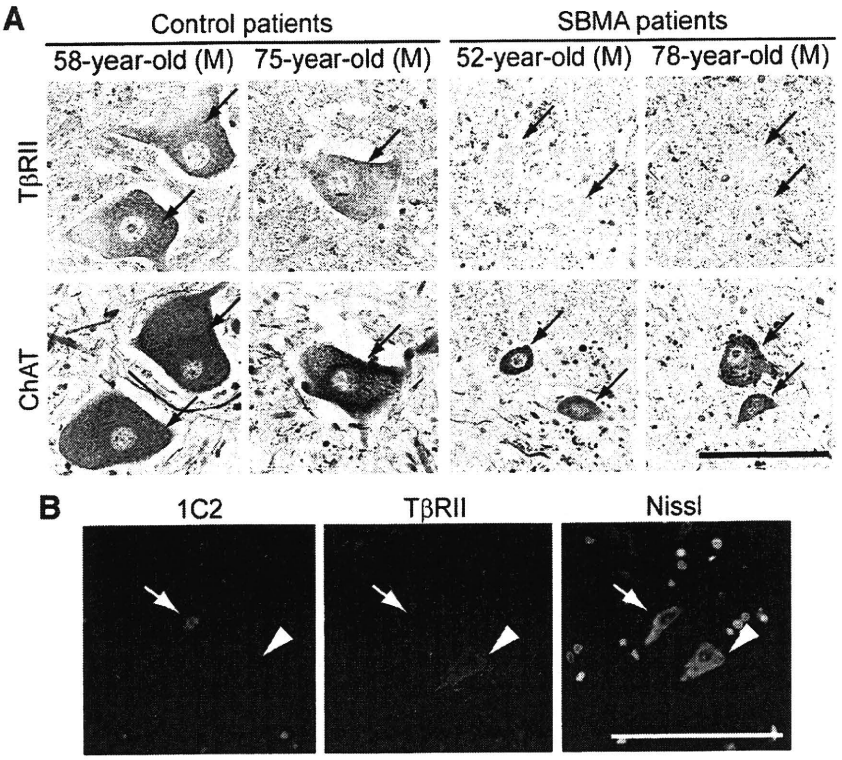

Figure 5. TβRII expression in SBMA patients. ***A***, Anti-TβRII immunohistochemistry in the spinal cords of an SBMA patients and control subjects. Arrows indicate identical neurons in each patient. ***B***, Immunofluorescence of the spinal cord from an SBMA patient using 1C2 in combination with an antibody against TβRII. Immunoreactivity for TβRII is detected in a 1C2-negative neuron (arrowhead) but decreased in a 1C2-positive neuron (arrow). Scale bars, 100 μm.

TGF-β signaling protects neurons against pathogenic AR toxicity

We next investigated whether the disruption of TGF-β signaling has a causative impact on polyglutamine-mediated neurotoxicity. To this end, we cotransfected SH-SY5Y cells with tAR24Q or tAR97Q and with or without a plasmid vector of TβRII. The cotransfection of TβRII increased the amount of pSmad2/3 in the SH-SY5Y cells expressing tAR97Q (Fig. 8*A*). Propidium iodide staining demonstrated that overexpression of TβRII inhibited the cell death induced by tAR97Q (Fig. 8*B*). Inclusion body formation, however, was not suppressed by the coexpression of TβRII (Fig. 8*C*), suggesting that TGF-β signaling attenuates the pathogenic AR-mediated cell damage without inhibiting the accumulation of abnormal polyglutamine protein.

To confirm these findings, we evaluated the effects of TβRII knock-down in SH-SY5Y cells. Suppression of TβRII expression using siRNA decreased nuclear pSmad2/3 and cytoplasmic TβRII (Fig. 8*D*) and significantly increased the number of dead cells detected by propidium iodide staining (control siRNA, 1.19 ± 0.62%; TβRII siRNA, 3.08 ± 0.54%; $p < 0.0005$; $n = 6$ per group). In addition, TβRII knock-down decreased cell viability to 77.4 ± 7.7% of control ($p < 0.05$; $n = 6$ per group). Given that both pharmacological and genetic suppression of TGF-β signaling was shown to induce degeneration of cultured neuroblastoma cells (Tesseur et al., 2006), our findings suggest that the mutant AR-mediated blockade of TGF-β signaling has cytotoxic effects on neuronal cells and thus is associated with polyglutamine-mediated cellular damage.

Discussion

TGF-β signal perturbation in polyglutamine-mediated neurodegeneration

The present study demonstrated that the accumulation of pathogenic AR proteins containing an expanded polyglutamine tract reduced the expression of TβRII and hampered the nuclear translocation of pSmad2/3 proteins. We also demonstrated that the deficiency in TGF-β signaling had causative effects on neuronal cell damage that was mitigated by the overexpression of TβRII. In support of our findings, the blockade of TGF-β signaling via neuron-specific expression of dominant-negative TβRII was shown to induce an age-dependent neurodegeneration and exacerbate neuropathology in a mouse model of Alzheimer's disease (AD) (Tesseur et al., 2006).

The TGF-β superfamily contains two subfamilies: the TGF-β/Activin/Nodal subfamily and the BMP/growth and differentiation factor/Muellerian inhibiting substance subfamily. TGF-β, a pleiotropic cytokine, regulates a diverse set of cellular responses, including proliferation, differentiation, migration, and apoptosis. TGF-β isoforms TGF-β1, -β2, and -β3 are expressed by both neurons and glial cells, and their receptors are expressed through-

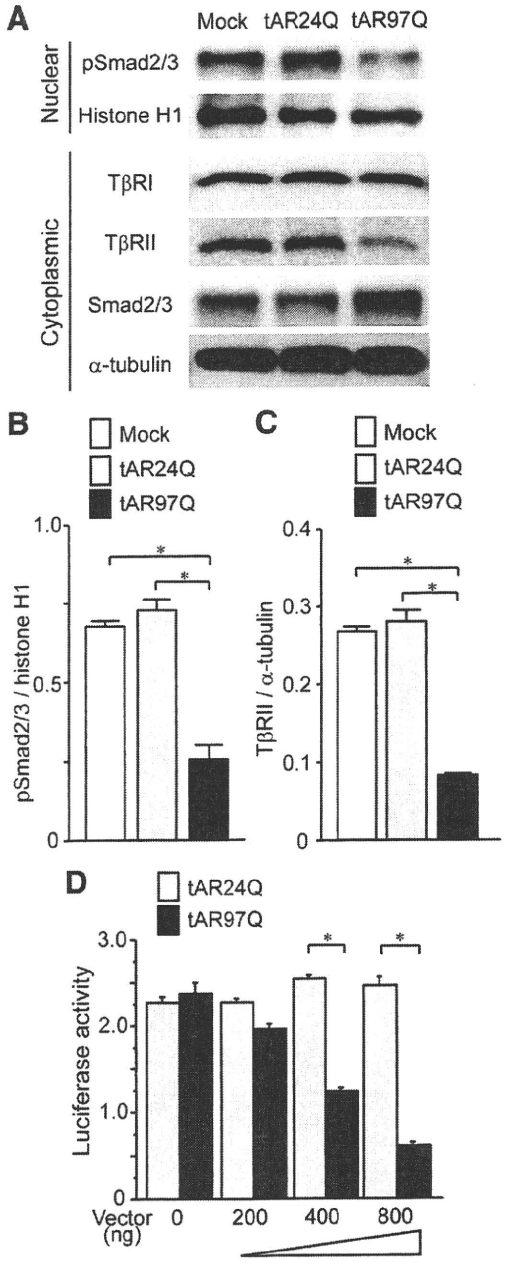

Figure 6. TGF-β-Smad2/3 pathway alteration in cellular model of SBMA. ***A***, Immunoblots of nuclear and cytoplasmic fractions from SH-SY5Y cells transfected with mock, tAR24Q, or tAR97Q vector. ***B***, Signal intensities of the pSmad2/3-immunoreactive bands from the nuclear fractions of SH-SY5Y cells ($n = 3$ per group). ***C***, Signal intensities of the TβRII-immunoreactive bands from the cytoplasmic fractions of SH-SY5Y cells ($n = 3$ per group). ***D***, The activity of luciferase, controlled by the TβRII promoter, in SH-SY5Y cells transfected with the indicated amounts of tAR24Q or tAR97Q ($n = 3$ per group). Error bars indicate SEM; $^*p < 0.01$.

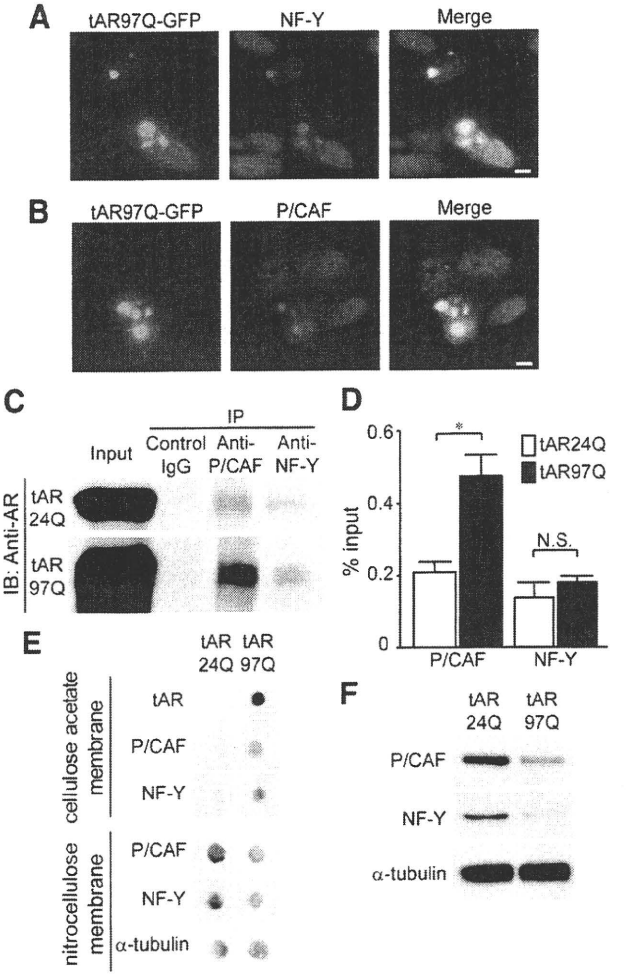

Figure 7. Pathogenic AR interferes with P/CAF and NF-Y. ***A***, Anti-NF-Y immunocytochemistry of SH-SY5Y cells expressing tAR97Q tagged with GFP. ***B***, Anti-P/CAF immunocytochemistry of SH-SY5Y cells expressing tAR97Q tagged with GFP. Scale bars, 10 μm. ***C***, Immunoprecipitation (IP)/immunoblot (IB) of soluble fraction from SH-SY5Y cells transfected with tAR24Q or with tAR97Q. Coimmunoprecipitation of tAR and the nuclear proteins P/CAF and NF-Y was detected. ***D***, Quantification of the amount of tAR proteins that are coimmunoprecipitated with P/CAF or NF-Y. Data are shown as a ratio to input. Error bars indicate SEM $^*p < 0.01$. ***E***, Filter trap assay of the protein lysate from SH-SY5Y cells transfected with tAR24Q or tAR97Q. ***F***, Immunoblots of soluble fraction from SH-SY5Y cells transfected with tAR24Q or tAR97Q.

out the CNS, including adult human neurons (Flanders et al., 1998). A number of studies have shown that the TGF-β-Smad2/3 pathway has potent neuroprotective effects. The observation that viral vector-mediated overexpression of TGF-β attenuates ischemic brain damage lends support to this view (Zhu et al., 2002). It was postulated that TGF-β signaling plays a fundamental role in neural activity through the regulation of synaptic function (Heupel et al., 2008). TGF-β was also shown to protect neurons from glutamate-mediated excitotoxicity, a putative molecular mechanism underlying the pathogenesis of a variety of neurodegenerative disorders, including polyglutamine diseases (Vivien and Ali, 2006; Fernandes et al., 2007). Furthermore, several studies demonstrated that TGF-β protects neurons from amyloid β-protein, the causative protein of AD (Flanders et al., 1998; Vivien and Ali, 2006). By contrast, genetic reduction of the TGF-β2 isoform was shown to induce a loss of dopaminergic neurons in mice, suggesting a link between TGF-β signaling and Parkinson's disease (Andrews et al., 2006). In the present study, we showed that the expression of TβRII and nuclear translocation of pSmad2/3 are suppressed in the affected neurons of patients with SBMA. A similar decrease in TβRII expression was also reported in AD patients, suggesting that this molecule plays an important role in various pathogeneses of neurodegeneration (Tesseur et al., 2006). Together, these findings indicate that the decreased expression of TβRII and the resulting perturbation of TGF-β signaling appear to underlie polyglutamine-dependent neurodegeneration in SBMA.

Transcriptional dysregulation in polyglutamine diseases

Dysregulation of cellular transcriptional machinery is considered the major molecular mechanism whereby pathogenic polyglu-

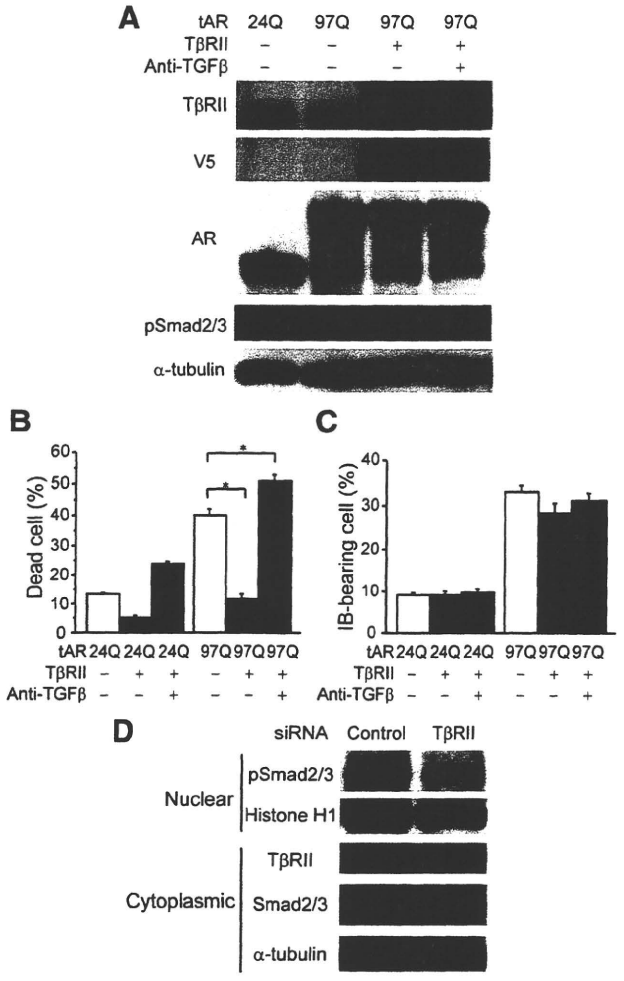

Figure 8. Modulation of TGF-β signaling in SH-SY5Y cells. ***A***, Immunoblots of total homogenates from SH-SY5Y cells transfected with tAR24Q or tAR97Q and with or without the coexpression of V5-tagged TβRII. Anti-TGF-β treatment was used to neutralize TGF-β signaling. ***B***, Frequency of cell death detected by propidium iodide staining in SH-SY5Y cells transfected with tAR24Q or tAR97Q ($n = 6$ per group) with or without the coexpression of TβRII ($n = 6$ per group). ***C***, Percentage of SH-SY5Y cells carrying inclusion bodies (IB) containing overexpressed AR protein ($n = 6$ per group). Error bars indicate SEM; $^*p < 0.01$. ***D***, Immunoblots of the nuclear and cytoplasmic fractions from SH-SY5Y cells transfected with siRNA against TβRII or control oligonucleotide.

tamine proteins induce neuron damage (Riley and Orr, 2006). However, it has yet to be elucidated which molecules are critically implicated in the pathophysiology of polyglutamine-dependent neurodegeneration. In the present study, we demonstrated that the transcription of TβRII, the mediator of TGF-β signaling, is dysregulated by the pathogenic AR protein. This finding was demonstrated in both cellular and animal models of SBMA. Furthermore, a similar finding was also revealed in an SBMA patient, suggesting that transcriptional perturbation of TβRII is a fundamental molecular event in SBMA.

Previous reports demonstrated that transcriptional alteration is an early change in the pathogenesis in mouse models of other polyglutamine diseases as well (Lin et al., 2000; Luthi-Carter et al., 2000). For example, the expression levels of various heat shock proteins were substantially decreased in animal models of SBMA, SCA3, and HD (Hay et al., 2004; Katsuno et al., 2005; Chou et al., 2008). Recent studies also demonstrated that pathogenic polyglutamine proteins repress the transcription of subunits of PGC-1 (peroxisome proliferator-activated receptor gamma coactivator-1), a transcriptional coactivator that regulates the expression of various nuclear-encoded mitochondrial proteins (Cui et al., 2006; Ranganathan et al., 2009). Moreover, we have demonstrated that pathogenic AR impairs retrograde axonal transport via transcriptional dysregulation of dynactin 1 in the mouse model of SBMA (Katsuno et al., 2006b). Given that activated Smads are retrogradely transported in motor axons, pathogenic AR-mediated axonal transport impairment may enhance TGF-β signal disruption in SBMA (Sanyal et al., 2004). Collectively, the pathogenic polyglutamine proteins perturb the transcription of a wide range of genes that play substantial roles in the maintenance of neuronal function, leading to neuronal dysfunction and cell death. Of note is that some of these transcriptional alterations are shared by different diseases, suggesting a common target of therapy development against polyglutamine-mediated neurodegenerative disorders.

Inhibition of histone deacetylase restores TGF-β signaling

The present study showed that the pathogenic AR aggregates sequestrate NF-Y and P/CAF, both of which regulate the transcription of TβRII (Park et al., 2002). This finding should be interpreted cautiously, since our cellular experiments were not performed using the full-length AR or on the gene's endogenous promoter. However, it has been particularly emphasized that a pivotal molecular event in polyglutamine diseases is an abnormal interaction between the respective pathogenic protein and nuclear proteins that regulate transcription. A recent study demonstrated that the components of NF-Y are sequestrated by the aggregates of pathogenic huntingtin in the brains of HD model mice (Yamanaka et al., 2008). P/CAF also interacts with an N-terminal fragment of huntingtin that contains an expanded polyglutamine tract (Steffan et al., 2001). Like other polyglutamine-interacting proteins, P/CAF possesses an intrinsic HAT activity that activates an NF-Y-dependent gene transcription (Jin and Scott, 1998). HDAC inhibition has been shown to upregulate this HAT activity of P/CAF, resulting in mitigation of polyglutamine-dependent neuropathology in a fly model of HD (Steffan et al., 2001). Although augmentation of histone acetylation was shown to attenuate neurodegeneration in several animal models of polyglutamine disease, the genes regulated by HDAC inhibitors in the affected neurons remained elusive (Minamiyama et al., 2004; Hockly et al., 2003; Ying et al., 2006). On the basis of our present findings, it appears reasonable to infer that the therapeutic effects of NaB, a potent HDAC inhibitor, in SBMA mice might stem from the restoration of TβRII expression.

Roles of TGF-β in non-neuronal cells

The present study showed that the pathway whereby Smad2/3 is phosphorylated and translocated to the nucleus is disrupted not only in the CNS but also in skeletal muscle of SBMA mice, suggesting that pathogenic AR disrupts TGF-β signaling in a cell type-independent manner. The TGF-β-Smad2/3 pathway functions in virtually all cell types, including muscle. TGF-β signaling was shown to have negative effects on muscle growth. Myostatin, a member of the TGF-β superfamily, has gained attention as a potential therapeutic target for myopathies, because genetic deletion of this factor results in an increased muscle volume (McPherron et al., 1997). Therefore, disrupted TGF-β signaling in skeletal muscle might play a protective role against muscular damage in SBMA mice. This protection, however, is likely not capable of compensating for the muscle damage due to the polyglutamine-induced degeneration of spinal motor neurons,

given the severe muscular atrophy present in the AR-97Q mice (Katsuno et al., 2002). In support of this view, a previous study showed that inhibition of myostatin has little effect on muscle damage in rodent models of ALS (Holzbaur et al., 2006).

The TGF-β-Smad2/3 pathway is also known to regulate the function of glial cells. However, a great deal of debate has been waged on how glial TGF-β signaling modulates the pathogenesis of neurodegeneration. TGF-β was shown to activate astrocytes and to protect against neuron damage caused by brain injury, while the overexpression of TGF-β in astrocytes promotes brain inflammation and AD-like microvascular degeneration (Flanders et al., 1998; Wyss-Coray et al., 2000). In polyglutamine diseases, the pathogenic proteins accumulate exclusively in neurons, suggesting that neuronal involvement is the primary molecular event triggering neurodegeneration. In accordance with this hypothesis, the present study suggests that the neuronal TGF-β-Smad2/3 pathway plays a substantial role in the molecular mechanisms underlying polyglutamine-mediated neurodegeneration, given that TGF-β signaling was disturbed both in transfected cultured neuronal cells and in neurons of diseased patients and mice.

In conclusion, the present study showed that polyglutamine-dependent neuron damage in SBMA is associated with the disruption of TGF-β signaling due to transcriptional dysregulation of TβRII. Our findings further suggest that restoration of the brain TGF-β-Smad2/3 pathway might be a potential therapeutic approach to polyglutamine-induced neurodegenerative diseases.

References

Adachi H, Kumiai A, Li M, Nakagomi Y, Niwa H, Do J, Sang C, Kobayashi Y, Doyu M, Sobue G (2001) Transgenic mice with an expanded CAG repeat controlled by the human AR promoter show polyglutamine nuclear inclusions and neuronal dysfunction without neuronal cell death. Hum Mol Genet 10:1039–1048.

Adachi H, Katsuno M, Minamiyama M, Sang C, Pagoulatos G, Angelidis C, Kusakabe M, Yoshiki A, Kobayashi Y, Doyu M, Sobue G (2003) Heat shock protein 70 chaperone overexpression ameliorates phenotypes of the spinal and bulbar muscular atrophy transgenic mouse model by reducing nuclear-localized mutant androgen receptor protein. J Neurosci 23:2203–2211.

Adachi H, Katsuno M, Minamiyama M, Waza M, Sang C, Nakagomi Y, Kobayashi Y, Tanaka F, Doyu M, Inukai A, Yoshida M, Hashizume Y, Sobue G (2005) Widespread nuclear and cytoplasmic accumulation of mutant androgen receptor in SBMA patients. Brain 128:659–670.

Adachi H, Waza M, Tokui K, Katsuno M, Minamiyama M, Tanaka F, Doyu M, Sobue G (2007) CHIP overexpression reduces mutant androgen receptor protein and ameliorates phenotypes of the spinal and bulbar muscular atrophy transgenic mouse model. J Neurosci 27:5115–5126.

Andrews ZB, Zhao H, Frugier T, Meguro R, Grattan DR, Koishi K, McLennan IS (2006) Transforming growth factor beta2 haploinsufficient mice develop age-related nigrostriatal dopamine deficits. Neurobiol Dis 21:568–575.

Banno H, Katsuno M, Suzuki K, Takeuchi Y, Kawashima M, Suga N, Takamori M, Ito M, Nakamura T, Matsuo K, Yamada S, Oki Y, Adachi H, Minamiyama M, Waza M, Atsuta N, Watanabe H, Fujimoto Y, Nakashima T, Tanaka F, et al. (2009) Phase 2 trial of leuprorelin in patients with spinal and bulbar muscular atrophy. Ann Neurol 65:140–150.

Brionne TC, Tesseur I, Masliah E, Wyss-Coray T (2003) Loss of TGF-beta 1 leads to increased neuronal cell death and microgliosis in mouse brain. Neuron 40:1133–1145.

Butler R, Bates GP (2006) Histone deacetylase inhibitors as therapeutics for polyglutamine disorders. Nat Rev Neurosci 7:784–796.

Chevalier-Larsen ES, O'Brien CJ, Wang H, Jenkins SC, Holder L, Lieberman AP, Merry DE (2004) Castration restores function and neurofilament alterations of aged symptomatic males in a transgenic mouse model of spinal and bulbar muscular atrophy. J Neurosci 24:4778–4786.

Chou AH, Yeh TH, Ouyang P, Chen YL, Chen SY, Wang HL (2008) Polyglutamine-expanded ataxin-3 causes cerebellar dysfunction of SCA3 transgenic mice by inducing transcriptional dysregulation. Neurobiol Dis 31:89–101.

Colavita A, Krishna S, Zheng H, Padgett RW, Culotti JG (1998) Pioneer axon guidance by UNC-129, a C. elegans TGF-beta. Science 281:706–709.

Cui L, Jeong H, Borovecki F, Parkhurst CN, Tanese N, Krainc D (2006) Transcriptional repression of PGC-1alpha by mutant huntingtin leads to mitochondrial dysfunction and neurodegeneration. Cell 127:59–69.

Dunah AW, Jeong H, Griffin A, Kim YM, Standaert DG, Hersch SM, Mouradian MM, Young AB, Tanese N, Krainc D (2002) Sp1 and TAFII130 transcriptional activity disrupted in early Huntington's disease. Science 296:2238–2243.

Fernandes HB, Baimbridge KG, Church J, Hayden MR, Raymond LA (2007) Mitochondrial sensitivity and altered calcium handling underlie enhanced NMDA-induced apoptosis in YAC128 model of Huntington's disease. J Neurosci 27:13614–13623.

Flanders KC, Ren RF, Lippa CF (1998) Transforming growth factor-betas in neurodegenerative disease. Prog Neurobiol 54:71–85.

Gatchel JR, Zoghbi HY (2005) Diseases of unstable repeat expansion: mechanisms and common principles. Nat Rev Genet 6:743–755.

Hay DG, Sathasivam K, Tobaben S, Stahl B, Marber M, Mestril R, Mahal A, Smith DL, Woodman B, Bates GP (2004) Progressive decrease in chaperone protein levels in a mouse model of Huntington's disease and induction of stress proteins as a therapeutic approach. Hum Mol Genet 13:1389–1405.

Heupel K, Sargsyan V, Plomp JJ, Rickmann M, Varoqueaux F, Zhang W, Krieglstein K (2008) Loss of transforming growth factor-beta 2 leads to impairment of central synapse function. Neural Dev 3:25.

Hockly E, Richon VM, Woodman B, Smith DL, Zhou X, Rosa E, Sathasivam K, Ghazi-Noori S, Mahal A, Lowden PA, Steffan JS, Marsh JL, Thompson LM, Lewis CM, Marks PA, Bates GP (2003) Suberoylanilide hydroxamic acid, a histone deacetylase inhibitor, ameliorates motor deficits in a mouse model of Huntington's disease. Proc Natl Acad Sci U S A 100:2041–2046.

Holzbaur EL, Howland DS, Weber N, Wallace K, She Y, Kwak S, Tchistiakova LA, Murphy E, Hinson J, Karim R, Tan XY, Kelley P, McGill KC, Williams G, Hobbs C, Doherty P, Zaleska MM, Pangalos MN, Walsh FS (2006) Myostatin inhibition slows muscle atrophy in rodent models of amyotrophic lateral sclerosis. Neurobiol Dis 23:697–707.

Jin S, Scotto KW (1998) Transcriptional regulation of the MDR1 gene by histone acetyltransferase and deacetylase is mediated by NF-Y. Mol Cell Biol 18:4377–4384.

Katsuno M, Adachi H, Kume A, Li M, Nakagomi Y, Niwa H, Sang C, Kobayashi Y, Doyu M, Sobue G (2002) Testosterone reduction prevents phenotypic expression in a transgenic mouse model of spinal and bulbar muscular atrophy. Neuron 35:843–854.

Katsuno M, Adachi H, Doyu M, Minamiyama M, Sang C, Kobayashi Y, Inukai A, Sobue G (2003) Leuprorelin rescues polyglutamine-dependent phenotypes in a transgenic mouse model of spinal and bulbar muscular atrophy. Nat Med 9:768–773.

Katsuno M, Sang C, Adachi H, Minamiyama M, Waza M, Tanaka F, Doyu M, Sobue G (2005) Pharmacological induction of heat-shock proteins alleviates polyglutamine-mediated motor neuron disease. Proc Natl Acad Sci U S A 102:16801–16806.

Katsuno M, Adachi H, Waza M, Banno H, Suzuki K, Tanaka F, Doyu M, Sobue G (2006a) Pathogenesis, animal models and therapeutics in spinal and bulbar muscular atrophy (SBMA). Exp Neurol 200:8–18.

Katsuno M, Adachi H, Minamiyama M, Waza M, Tokui K, Banno H, Suzuki K, Onoda Y, Tanaka F, Doyu M, Sobue G (2006b) Reversible disruption of dynactin 1-mediated retrograde axonal transport in polyglutamine-induced motor neuron degeneration. J Neurosci 26:12106–12117.

La Spada AR, Wilson EM, Lubahn DB, Harding AE, Fischbeck KH (1991) Androgen receptor gene mutations in X-linked spinal and bulbar muscular atrophy. Nature 352:77–79.

Li M, Miwa S, Kobayashi Y, Merry DE, Yamamoto M, Tanaka F, Doyu M, Hashizume Y, Fischbeck KH, Sobue G (1998) Nuclear inclusions of the androgen receptor protein in spinal and bulbar muscular atrophy. Ann Neurol 44:249–254.

Lin X, Antalffy B, Kang D, Orr HT, Zoghbi HY (2000) Polyglutamine expansion down-regulates specific neuronal genes before pathologic changes in SCA1. Nat Neurosci 3:157–163.

Luthi-Carter R, Strand A, Peters NL, Solano SM, Hollingsworth ZR, Menon AS, Frey AS, Spektor BS, Penney EB, Schilling G, Ross CA, Borchelt DR,

Tapscott SJ, Young AB, Cha JH, Olson JM (2000) Decreased expression of striatal signaling genes in a mouse model of Huntington's disease. Hum Mol Genet 9:1259–1271.

McPherron AC, Lawler AM, Lee SJ (1997) Regulation of skeletal muscle mass in mice by a new TGF-beta superfamily member. Nature 387:83–90.

Minamiyama M, Katsuno M, Adachi H, Waza M, Sang C, Kobayashi Y, Tanaka F, Doyu M, Inukai A, Sobue G (2004) Sodium butyrate ameliorates phenotypic expression in a transgenic mouse model of spinal and bulbar muscular atrophy. Hum Mol Genet 13:1183–1192.

Niwa H, Yamamura K, Miyazaki J (1991) Efficient selection for high-expression transfectants with a novel eukaryotic vector. Gene 108:193–199.

Nucifora FC Jr, Sasaki M, Peters MF, Huang H, Cooper JK, Yamada M, Takahashi H, Tsuji S, Troncoso J, Dawson VL, Dawson TM, Ross CA (2001) Interference by huntingtin and atrophin-1 with cbp-mediated transcription leading to cellular toxicity. Science 291:2423–2428.

Palhan VB, Chen S, Peng GH, Tjernberg A, Gamper AM, Fan Y, Chait BT, La Spada AR, Roeder RG (2005) Polyglutamine-expanded ataxin-7 inhibits STAGA histone acetyltransferase activity to produce retinal degeneration. Proc Natl Acad Sci U S A 102:8472–8477.

Park SH, Lee SR, Kim BC, Cho EA, Patel SP, Kang HB, Sausville EA, Nakanishi O, Trepel JB, Lee BI, Kim SJ (2002) Transcriptional regulation of the transforming growth factor beta type II receptor gene by histone acetyltransferase and deacetylase is mediated by NF-Y in human breast cancer cells. J Biol Chem 277:5168–5174.

Peart MJ, Smyth GK, van Laar RK, Bowtell DD, Richon VM, Marks PA, Holloway AJ, Johnstone RW (2005) Identification and functional significance of genes regulated by structurally different histone deacetylase inhibitors. Proc Natl Acad Sci U S A 102:3697–3702.

Ranganathan S, Harmison GG, Meyertholen K, Pennuto M, Burnett BG, Fischbeck KH (2009) Mitochondrial abnormalities in spinal and bulbar muscular atrophy. Hum Mol Genet 18:27–42.

Riley BE, Orr HT (2006) Polyglutamine neurodegenerative diseases and regulation of transcription: assembling the puzzle. Genes Dev 20:2183–2192.

Sadri-Vakili G, Bouzou B, Benn CL, Kim MO, Chawla P, Overland RP, Glajch KE, Xia E, Qiu Z, Hersch SM, Clark TW, Yohrling GJ, Cha JH (2007) Histones associated with downregulated genes are hypo-acetylated in Huntington's disease models. Hum Mol Genet 16:1293–1306.

Sanyal S, Kim SM, Ramaswami M (2004) Retrograde regulation in the CNS; neuron-specific interpretations of TGF-beta signaling. Neuron 41:845–848.

Shi Y, Massague J (2003) Mechanisms of TGF-beta signaling from cell membrane to the nucleus. Cell 113:685–700.

Steffan JS, Bodai L, Pallos J, Poelman M, McCampbell A, Apostol BL, Kazantsev A, Schmidt E, Zhu YZ, Greenwald M, Kurokawa R, Housman DE, Jackson GR, Marsh JL, Thompson LM (2001) Histone deacetylase inhibitors arrest polyglutamine-dependent neurodegeneration in Drosophila. Nature 413:739–743.

Takeyama K, Ito S, Yamamoto A, Tanimoto H, Furutani T, Kanuka H, Miura M, Tabata T, Kato S (2002) Androgen-dependent neurodegeneration by polyglutamine-expanded human androgen receptor in Drosophila. Neuron 35:855–864.

Tesseur I, Zou K, Esposito L, Bard F, Berber E, Can JV, Lin AH, Crews L, Tremblay P, Mathews P, Mucke L, Masliah E, Wyss-Coray T (2006) Deficiency in neuronal TGF-beta signaling promotes neurodegeneration and Alzheimer's pathology. J Clin Invest 116:3060–3069.

Tokui K, Adachi H, Waza M, Katsuno M, Minamiyama M, Doi H, Tanaka K, Hamazaki J, Murata S, Tanaka F, Sobue G (2009) 17-DMAG ameliorates polyglutamine-mediated motor neuron degeneration through well-preserved proteasome function in an SBMA model mouse. Hum Mol Genet 18:898–910.

Vivien D, Ali C (2006) Transforming growth factor-beta signalling in brain disorders. Cytokine Growth Factor Rev 17:121–128.

Waza M, Adachi H, Katsuno M, Minamiyama M, Sang C, Tanaka F, Inukai A, Doyu M, Sobue G (2005) 17-AAG, an Hsp90 inhibitor, ameliorates polyglutamine-mediated motor neuron degeneration. Nat Med 11:1088–1095.

Wyss-Coray T, Lin C, Sanan DA, Mucke L, Masliah E (2000) Chronic overproduction of transforming growth factor-beta1 by astrocytes promotes Alzheimer's disease-like microvascular degeneration in transgenic mice. Am J Pathol 156:139–150.

Yamanaka T, Miyazaki H, Oyama F, Kurosawa M, Washizu C, Doi H, Nukina N (2008) Mutant Huntingtin reduces HSP70 expression through the sequestration of NF-Y transcription factor. EMBO J 27:827–839.

Ying M, Xu R, Wu X, Zhu H, Zhuang Y, Han M, Xu T (2006) Sodium butyrate ameliorates histone hypoacetylation and neurodegenerative phenotypes in a mouse model for DRPLA. J Biol Chem 281:12580–12586.

Zheng X, Zugates CT, Lu Z, Shi L, Bai JM, Lee T (2006) Baboon/dSmad2 TGF-beta signaling is required during late larval stage for development of adult-specific neurons. EMBO J 25:615–627.

Zhu Y, Yang GY, Ahlemeyer B, Pang L, Che XM, Culmsee C, Klumpp S, Krieglstein J (2002) Transforming growth factor-beta 1 increases bad phosphorylation and protects neurons against damage. J Neurosci 22:3898–3909.

Behavioural Brain Research 210 (2010) 184–190

Contents lists available at ScienceDirect

Behavioural Brain Research

journal homepage: www.elsevier.com/locate/bbr

Research report

Oral supplementation with Leu-Ile, a hydrophobic dipeptide, prevents the impairment of memory induced by amyloid beta in mice via restraining the hyperphosphorylation of extracellular signal-regulated kinase

Tursun Alkam[a,b,c], Atsumi Nitta[a,e], Yoko Furukawa-Hibi[a], Minae Niwa[a,c], Hiroyuku Mizoguchi[a,d], Kiyofumi Yamada[a,e], Toshitaka Nabeshima[a,c,e,*]

[a] Department of Neuropsychopharmacology & Hospital Pharmacy, Nagoya University Graduate School of Medicine, Nagoya 466-8560, Japan
[b] Department of Basic Medicine, College of Traditional Uighur Medicine, Hotan 848-000, China
[c] Department of Chemical Pharmacology, Graduate School of Pharmaceutical Science, Meijo University, Nagoya 468-8503, Japan
[d] Futuristic Environmental Simulation Center, Research Institute of Environmental Medicine, Nagoya University, Nagoya 464-8601, Japan
[e] Japanese Drug Organization of Appropriate Use and Research, Nagoya 468-0069, Japan

ARTICLE INFO

Article history:
Received 15 November 2009
Received in revised form 6 February 2010
Accepted 12 February 2010
Available online 19 February 2010

Keywords:
Amyloid beta (25–35)
Extracellular signal-regulated kinase
Inducible nitric oxide synthase
Protein nitration
Novel object recognition memory

ABSTRACT

Restraining the toxic pathways of amyloid beta peptide (Aβ) by daily supplementation with dietary products has been shown effective in preventing cognitive decline. In this study, we examined the effects of the orally administered Leu-Ile, a hydrophobic dipeptide, on the neurotoxicity of $A\beta_{25-35}$ in mice. Chronic daily treatment with Leu-Ile prevented the $A\beta_{25-35}$-induced protein nitration and impairment of novel object recognition memory in mice. Protein nitration in the hippocampus induced by $A\beta_{25-35}$ was associated with the hyperphosphorylation of extracellular signal-regulated kinase (ERK) which was found responsible for the over-expression of inducible nitric oxide synthase. Sub-chronic treatment with Leu-Ile prevented the $A\beta_{25-35}$-induced hyperphosphorylation of ERK and protein nitration in the hippocampus. The results suggested that with the protective property against the neurotoxicity of $A\beta_{25-35}$, Leu-Ile could be considered as a candidate for the dietary supplementation in the prevention of Aβ-related impairment of recognition memory.

1. Introduction

Delaying or preventing the cognitive disorders in the elderly is a global imperative. The most studied cognitive disorder in modern history is Alzheimer's disease (AD), thanks to the assumption of amyloid beta peptide (Aβ) as the main player in its multifactor pathology. The recent advances in the understandings of the pathogenesis of AD propose the disruption of the neurotoxic pathways of Aβ as the main preventive approach to delay or control the progression of the disease [64,68]. However, the options for the preventive treatment are extremely limited due to the multifactor pathology that makes the management of AD a more complex process [16,31,38,43]. Further, the developments of new drugs take years before the general clinical application. Therefore, the oral supplements with the protective effects against Aβ should be considered for the immediate preventive treatment of AD.

The positive associations of the levels of cerebral Aβ and oxidative damage with the progression of the cognitive decline in the early stages of AD suggest an antioxidant- intervention strategy to delay the development of the disease [7,9,11,17,18,30,35,41,55,66]. In support, growing body of recent findings supports the use of dietary supplements with antioxidant capacity to retard the Aβ-associated decline of cognitive function in both animal and human [26,48,53,67,69].

The most abundant Aβ species in the brain of AD is $A\beta_{1-40}$. $A\beta_{1-40}$ can be truncated into a more toxic fragment $A\beta_{25-35}$ in the brain of AD [22]. $A\beta_{25-35}$ possesses the strongest oxidative capacity among all Aβ species [10,47,54]. Therefore, many recent studies applied $A\beta_{25-35}$ to investigate the usefulness of anti-oxidants in the protection against Aβ-induced impairment of memory in mice [12,32,61]. We have previously reported that restraining oxidative pathways of $A\beta_{25-35}$ that enhances nitration of protein (an indicator of oxidative damage) could prevent the impairments of memory in mice [3,4]. We have also reported that Leu-Ile, a hydrophobic dipeptide, protects against a neuronal damage induced by a strong oxidative reagent, 6-hydroxydopamine (6-OHDA) [39]. Therefore,

* Corresponding author at: Department of Chemical Pharmacology, Graduate School of Pharmaceutical Science, Meijo University, Nagoya 468-8503, Japan. Tel.: +81 52 835 2735; fax: +81 52 839 2735.
E-mail addresses: tnabeshi@med.nagoya-u.ac.jp, tnabeshi@ccmfs.meijo-u.ac.jp (T. Nabeshima).

0166-4328/$ – see front matter © 2010 Elsevier B.V. All rights reserved.
doi:10.1016/j.bbr.2010.02.028

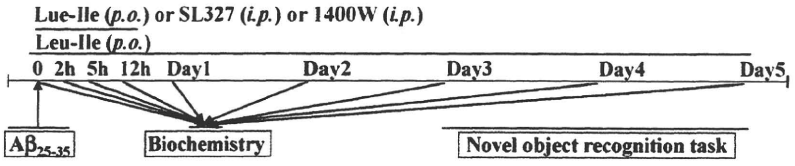

Fig. 1. Experimental schedule.

in this study, we have examined whether the oral supplementation with Leu-Ile could protect against $A\beta_{25-35}$-induced impairment of memory in mice. The results indicated that the oral treatment with Leu-Ile could prevent the enhanced nitration of protein in the hippocampus and the resultant impairment of novel object recognition memory in mice via restraining the hyperphosphorylation of extracellular signal-regulated kinase (ERK) induced by $A\beta_{25-35}$.

2. Materials and methods

2.1. Animals

Male, 5 weeks old ICR mice (Nihon SLC Co., Shizuoka, Japan), were used. The animals were housed in a controlled environment (23 ± 1 °C, 50 ± 5% humidity) and allowed food and water ad lib. The room lights were kept on between 8:00 a.m. and 8:00 p.m. All experiments were performed in accordance with the Guidelines for Animal Experiments of Nagoya University Graduate School of Medicine. The procedures involving animals and their care conformed to the Guidelines for Proper Conduct of Animal Experiments (Science Council of Japan, 2006).

2.2. Treatment and experimental design

$A\beta_{25-35}$ (Bachem, Bubendorf, Switzerland) was dissolved in sterile double-distilled water at the concentration of 1 mg/ml and stored at −20 °C before use and incubated for aggregation at 37 °C for 4 days before the injection [32]. The double distilled water was also incubated at the same condition as control. Incubated $A\beta_{25-35}$ (3 μg/3 μl) or incubated distilled water (control) (3 μl) was i.c.v.-injected as described previously [4,32]. Briefly, a microsyringe with a 28-gauge stainless-steel needle 3.0 mm long was used for all experiments. Mice were anesthetized lightly with ether, and the needle was inserted unilaterally 1 mm to the right of the midline point equidistant from each eye, at an equal distance between the eyes and the ears and perpendicular to the plane of the skull. A single-shot of the same volume (3 μl) of peptide or vehicle was delivered gradually within 3 s. Mice exhibited normal behaviour within 1 min after injection. The administration site was confirmed in preliminary experiments. Neither insertion of the needle nor the volume of injection had a significant influence on survival, and behavioural responses or cognitive functions.

Leu-Ile (Kokusan Chemical Co., Ltd., Tokyo, Japan) was dissolved in saline and was administered by either intraperitoneally (*i.p.*) or perorally (*p.o.*) at different doses which were decided according to a pilot study (unpublished data). The selective ERK inhibitor, α-[amino[(4-aminophenyl)thio]methylene]-2-(trifluoromethyl)-benzeneacetonitrile (SL327) (Sigma), was dissolved in dimethyl sulfoxide (DMSO). The selective inhibitor of iNOS, 1400W dihydrochloride (Sigma), was dissolved in normal saline (0.9% NaCl). The drugs were given by intraperitoneal (*i.p.*)-injection at indicated doses in a volume of 20 μl/10 g body weight [42].

The schedule of administration of peptides and drugs as well as biochemical and behavioral investigations is shown in Fig. 1.

2.3. Real-time reverse transcription-polymerase chain reaction

Mice were decapitated at the indicated time-points after the *i.c.v.*-injection of $A\beta_{25-35}$. The hippocampi were removed on ice-cold glass plate and stored at −80 °C. The hippocampal tissue was homogenized and total RNA was extracted using an RNeasy total RNA isolation kit, following the supplier's protocol (Qiagen, Valencia, CA). cDNA was synthesized by using a Superscript™ reverse transcriptase kit (Invitrogen, Carlsbad, CA). The primer sequences were given below: for TNF-α (Gene Bank access: NM_023517), forward primer: 5′-CTTTCGGTTGCTCTTTGGTTGAG-3′; reverse primer: 5′-GCAGCTCTGTCTGTTGGATCAG-3′; TaqMan probe: TGCGACAGCACAAGTCACAGCCCC; for the brain-derived neurotrophic factor (BDNF) (Gene Bank access: BC034862), forward primer: 5′-GCAAACATGTCTATGAGGGTTCG-3′; reverse primer: 5′-ACTCGCTAATACTGTCACACACG-3′; TaqMan probe: ACTCCGACCCTGCCCGCCGT; for glial cell-derived neurotrophic factor (GDNF) (Gene Bank access: NM_010275), forward primer: 5′-GAAGAGAGAGGAATCGGCAGG-3′; reverse primer: 5′-TGGCCTCTGCGACCTTTC-3′; TaqMan probe: AGCTGCCAGCCCAGAGAATTCCAGAG; For all, the experimental amplification protocol consisted of a first round at 95 °C for 3 min and then 30 cycles of denaturation at 95 °C for 60 s, annealing at 60 °C for 60 s, and extension at 72 °C for 1 min, with a final extension reaction carried out at 72 °C for 10 min. PCR was carried out on Bio-Rad iCycler iQ™ real-time PCR detection system (Bio-Rad Laboratories, Hercules, CA). The signal was detected according to the manufacturer's instructions. The expression levels were calculated as described previously [5].

2.4. Western blotting

Animals were decapitated at the indicated time-points after the injection of $A\beta_{25-35}$. The hippocampi were removed on ice-cold glass plate and stored at −80 °C. The hippocampal tissues were homogenized as described previously [3]. Briefly, the hippocampal tissues were homogenized in ice-cold extraction buffer (150 μl of 20 mM trizma hydrochloride buffer (pH 7.6) containing 150 mM sodium chloride, 2 mM EDTA·2Na, 50 mM sodium fluoride, 1 mM sodium vanadate, 1% Nonidet P-40, 1% sodium deoxycholate, 0.1% sodium dodecyl sulfate (SDS), 1 mg/ml pepstatin, 1 mg/ml aprotinin, and 1 mg/ml leupeptin). Equal amounts of protein, 20 μg/lane, were resolved by a 10% SDS-polyacrylamide gel electrophoresis, and then transferred electrophoretically to a polyvinylidene difluoride membrane (Millipore, Billerica, MA). Membranes were incubated in 3% skim milk (for nitrotyrosine and iNOS) or 3% bovine serum albumin (for phospho-proteins) in phosphate-buffered saline containing 0.05% (v/v) Tween 20 for 2 h at room temperature. Then the membranes were independently incubated at 4 °C overnight with anti-nitrotyrosine mouse monoclonal 1A6 antibody (Millipore, Billerica, MA), anti-iNOS rabbit polyclonal antibody (Upstate Biotechnology, Lake Placid, NY), anti-ERK(1/2) phospho-threonine202/tyrosine204 (p-ERK) rabbit antibody (Cell Signaling Technologies, Beverley, MA), anti-ERK(1/2) rabbit antibody (Cell Signaling Technologies, Beverley, MA), phospho and total anti-Jun N-terminal kinase (JNK) rabbit antibody (Santa Cruz Biotechnology Inc., Santa Crutz, CA), phospho and total anti-p38 MAPK rabbit antibody (Santa Cruz Biotechnology Inc., Santa Crutz, CA), and anti-β-actin goat antibody (Santa Cruz Biotechnology Inc., Santa Crutz, CA) were used. After washes, membranes were incubated with horseradish peroxidase-labeled anti-mouse IgG or anti-rabbit IgG (Kirkegaard & Perry Laboratories, Baltimore, MD) or with donkey anti-goat IgG secondary antibody (Santa Cruz Biotechnology Inc., Santa Crutz, CA). Immunoreactive complexes on the membrane were detected using Western blotting detection reagents (Amersham Biosciences Inc., Piscataway, NJ) according to the manufacturer's instructions, and exposed to X-ray film. The intensity of each protein band on the film was analyzed with the Atto Densitograph 4.1 system (Atto, Tokyo, Japan), and was corrected with the corresponding β-actin level. The results were expressed as the percentage of that of the control.

2.5. Novel object recognition task

This task, based on the spontaneous tendency of rodents to explore a novel object more often than a familiar one [15], was performed during Day 3 to Day 5 after the *i.c.v.*-injection of $A\beta_{25-35}$ (Day 0) as described previously [4]. A plastic chamber (35 cm × 35 cm × 35 cm) was used in low light condition during the light phase of the light/dark cycle. The general procedure consisted of three different phases: a habituation phase, an acquisition phase, and a retention phase. On the 1st day (habituation phase), mice were individually subjected to a single familiarization session of 10 min, during which they were introduced in the empty arena, in order to become familiar with the apparatus. On the 2nd day (acquisition phase) animals were subjected to a single 10-min session, during which floor-fixed two objects (A and B) were placed in a symmetric position from the centre of the arena, 15 cm from each and 8 cm from the nearest wall. The two objects, made of the same wooden material with the similar color and smell, were different in shape but identical in size. Mice were allowed to explore the objects in the open field. A preference index for each mouse was expressed as a ratio of the amount of time spent exploring object A (TA × 100)/(TA + TB), where TA and TB are the time spent on exploring object A and object B, respectively. On the 3rd day (retention phase), mice were allowed to explore the open field in the presence of two objects: the familiar object A and a novel object C in different shape but in similar color and size (A and C). A recognition index, calculated for each mouse, was expressed as the ratio (TC × 100)/(TA + TC), where TA and TC are the time spent during retention phase on object A and object C, respectively. The time spent exploring the object (nose pointing toward the object at a distance ≤1 cm) was recorded by hand.

2.6. Statistical analyses

The results are expressed as the mean ± S.E. Statistical significance was determined with one-way ANOVA followed by the Bonferroni multiple comparisons test. $p < 0.05$ was taken as a significant level of difference.

3. Results

3.1. Leu-Ile prevented impairment of memory via blocking protein nitration induced by $A\beta_{25-35}$

Daily treatments with Leu-Ile was commenced immediately before the *i.c.v.*-injection of $A\beta_{25-35}$ (Day 0) and continued (once a day) until Day 5. During the Day 3–5, the novel object recognition task was performed. During the acquisition phase of the task, all groups explored the two different objects for a similar amount of time (Fig. 2A). No differences among groups were observed concerning overall object exploration when different doses of Leu-Ile were administered. During the retention phase, the $A\beta_{25-35}$-injected mice did not discriminate the novel and familiar objects, and displayed a significantly decreased exploration to the new object in comparison with the control mice. Leu-Ile enhanced the new object discrimination ability of $A\beta_{25-35}$-injected mice (Fig. 2B). We have previously reported that chronic treatment with Leu-Ile can boost the mRNA levels of the brain-derived neurotrophic factor (BDNF), the glial cell line-derived neurotrophic factor (GDNF), and tumor necrosis factor-alpha (TNF-α) in the striatum of mice treated with 6-OHDA or methamphetamine [39,40]. It was therefore assumed that the enhanced expression of these factors by Leu-Ile might contribute to the amelioration of the $A\beta_{25-35}$-induced impairment of memory. As shown (Fig. 2C–E), the daily oral treatment with Leu-Ile did not change the mRNA levels of GDNF, BDNF, and TNF-α in the hippocampus (Day 5) of mice that received $A\beta_{25-35}$ injection (Day 0). The acute treatment with Leu-Ile did not change the mRNA levels of these factors in the hippocampus (data not shown). Daily treatment with Leu-Ile prevented $A\beta_{25-35}$-induced extensive nitration of hippocampal protein (indicated as nitrotyrosine) that appeared in a single band (Day 5) (Fig. 2F). We have previously confirmed the singularity of the band and identified the nitrated protein as neurofilament-L whose nitration is well associated with the impairment of memory in mice [3]. The above results suggested that the protective effect of Leu-Ile on the impairment of memory in mice could be due to the prevention of nitration of protein induced by $A\beta_{25-35}$.

3.2. Leu-Ile prevented $A\beta_{25-35}$-induced hyperphosphorylation of ERK

The intensity of nitration of proteins could be indicated by the elevation of the activity and protein level of inducible nitric oxide synthase (iNOS) induced by Aβ [37,52,58]. Both the activity and expression of iNOS are up-regulated by the persistent hyper-

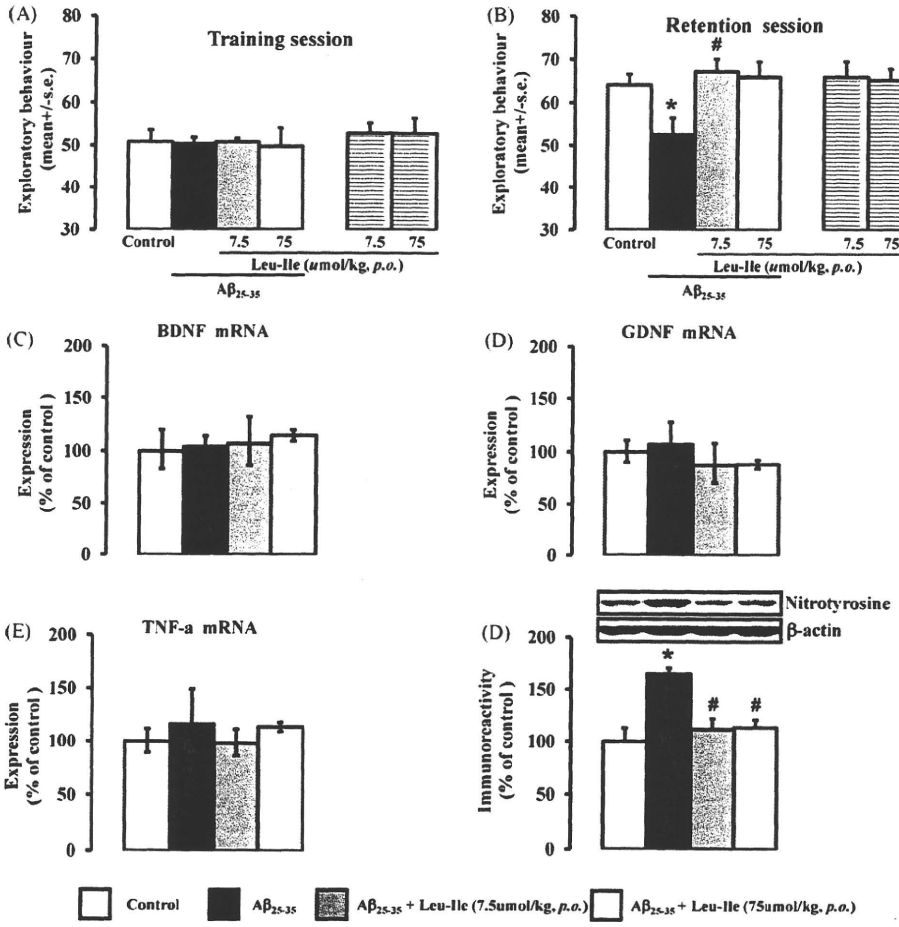

Fig. 2. Leu-Ile protects against memory impairment and hippocampal protein nitration induced by $A\beta_{25-35}$. Leu-Ile was administered immediately *p.o.* before the *i.c.v.*-injection of $A\beta_{25-35}$ (Day 0) and continued daily for next 5 consecutive days. (A and B) On Day 3–5 after the injection of $A\beta_{25-35}$, mice were subjected to the novel object recognition task. On training session (Day 4), neither $A\beta_{25-35}$ nor Leu-Ile affected the overall object exploration of mice. On retention session (Day 5), $A\beta_{25-35}$-injected mice displayed impairment of recognition memory. Treatment with Leu-Ile prevented the impairment of memory induced by $A\beta_{25-35}$. (C–E) Leu-Ile had no effect on the mRNA expression of GDNF, BDNF, and TNF-α in the hippocampus of $A\beta_{25-35}$-injected mice. (F) Increased nitration of hippocampal protein was found in $A\beta_{25-35}$-injected mice. Leu-Ile prevented the enhanced nitration of protein in the hippocampus induced by $A\beta_{25-35}$. Data were presented as the mean ± S.E., $n = 10$ for A and B; $n = 4$ for C–F; $^{*}p < 0.05$ vs. control. $^{\#}p < 0.05$ vs. $A\beta_{25-35}$. $A\beta_{25-35}$: Amyloid beta 25–35, GDNF: glia-drived neurotrophic factor, BDNF: brain-drived neurotrophic factor, TNF-α: tumor necrosis factor alpha.

phosphorylation of ERK, a member of mitogen activated protein kinase (MAPK) family [44,71]. We have previously reported the time dependent expression of iNOS mRNA by $A\beta_{25-35}$ [5]. We have therefore now examined the involvement of ERK and over-expression of iNOS protein in the neurotoxicity of $A\beta_{25-35}$. $A\beta_{25-35}$ enhanced the expression of iNOS protein in a time-dependent manner (Fig. 3A and B). $A\beta_{25-35}$ also persistently enhanced the phosphorylation of ERK at the time points that precedes the enhanced expression of iNOS (Fig. 3A and B). The phosphorylation of other members of MAPK family including c-Jun N-terminal kinase (JNK) and p38 were not affected by $A\beta_{25-35}$ (Fig. 3A and B). To examine the involvement of ERK in the induction of iNOS, we applied SL327, a selective inhibitor of the phosphorylation of ERK [42,63]. Since the inhibitory dose of SL327 (30 mg/kg, *i.p.*), which brings on the hypophosphorylation of ERK, did not prevent the impairment of memory induced by $A\beta_{25-35}$ and even impaired the memory in naïve mice (data not shown), we attempted to examine the sub-inhibitory dose of SL327 to restrain the $A\beta_{25-35}$-induced hyperphosphorylation of ERK without bringing on the hypophosphorylation. The lowest sub-inhibitory dose of SL327 (15 mg/kg, *i.p.*) on phosphorylation of ERK was identified in naïve mice (Fig. 3C). Treatment with SL327 at two doses (the inhibitory and sub-inhibitory), immediately before and 12 h after the *i.c.v.*-injection (at 0 h) of $A\beta_{25-35}$, almost identically prevented the enhanced expression of iNOS on Day 1 (at 24 h) (Fig. 3D). Selective inhibition of the activity of iNOS, with 1400W, prevented protein nitration on Day 1 induced by $A\beta_{25-35}$ (Fig. 3E). The results came with an agreement with the reports on the selective involvement of hyperphosphorylation of ERK in the regulation of iNOS [71] and in the oxidative toxicity of Aβ [1,13,24,33]. Treatment with SL327 (15 mg/kg, *i.p.*) immediately before and 12 h after the *i.c.v.*-injection of $A\beta_{25-35}$ prevented the hyperphosphorylation of ERK (on Day 1), protein nitration and impairment of memory (on Day 5) (Fig. 4A–D). The preventive effects of treatment with

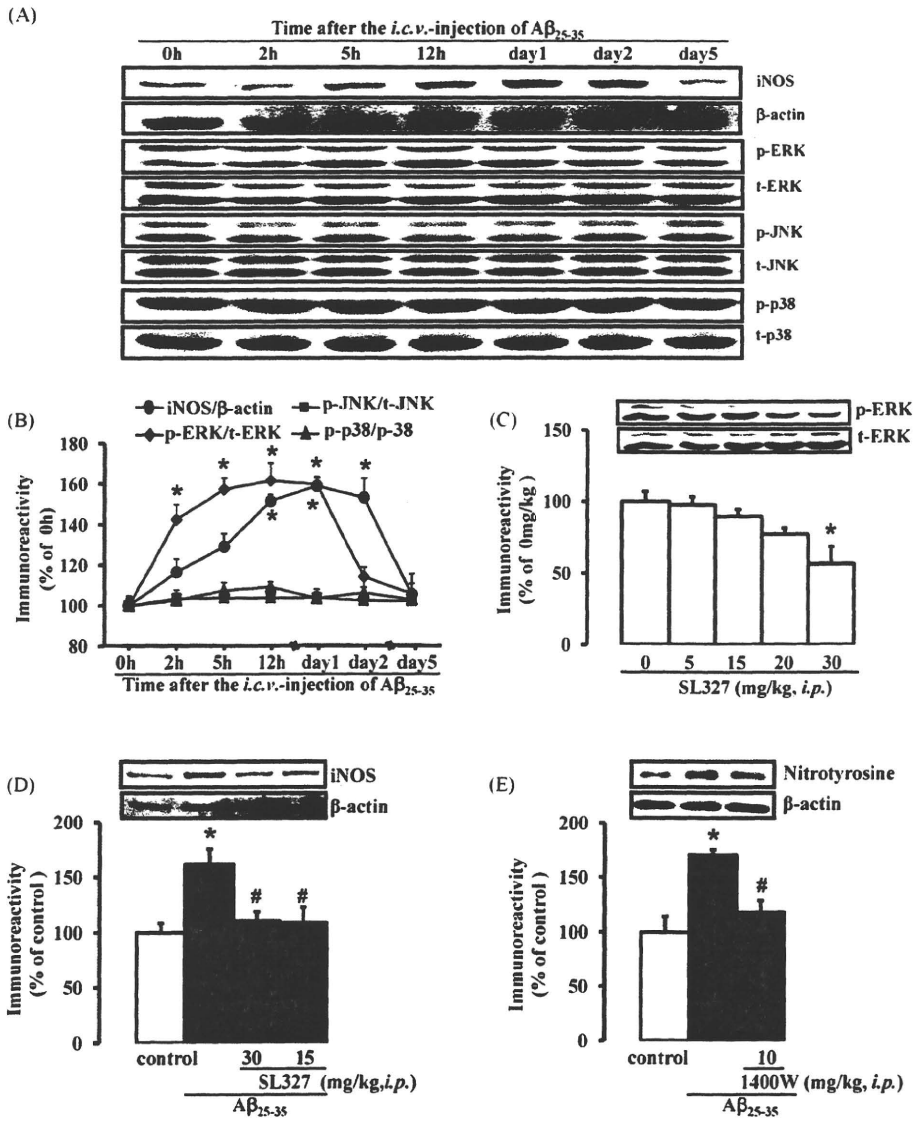

Fig. 3. Hyperphosphorylation of ERK is involved in the nitration of protein induced by $A\beta_{25-35}$. (A and B) At different time points after the *i.c.v.*-injection of $A\beta_{25-35}$ (0 h), the expression of iNOS and the phosphorylation levels of ERK, JNK, and p38 in the hippocampus were examined. Hyperphosphorylation of ERK precedes the enhanced expression of iNOS. The phosphorylation levels of JNK and p38 were not changed. (C and D) SL327, a selective inhibitor of ERK, was *i.p.*-injected at the inhibitory and sub-inhibitory doses immediately before and 12 h after the *i.c.v.*-injection of $A\beta_{25-35}$. Both doses prevented the enhanced expression of iNOS (at 24 h, or on Day 1) induced by $A\beta_{25-35}$. (E) Selective inhibition of iNOS by 1400W immediately before and 12 h after the *i.c.v.*-injection of $A\beta_{25-35}$ prevented the enhanced nitration of protein in the hippocampus. Data were presented as the mean ± S.E.; $n = 4$, $^{*}p < 0.05$ vs. control or 0 h or 0 mg/kg (SL327). $^{\#}p < 0.05$ vs. $A\beta_{25-35}$. $A\beta_{25-35}$: Amyloid beta 25–35.

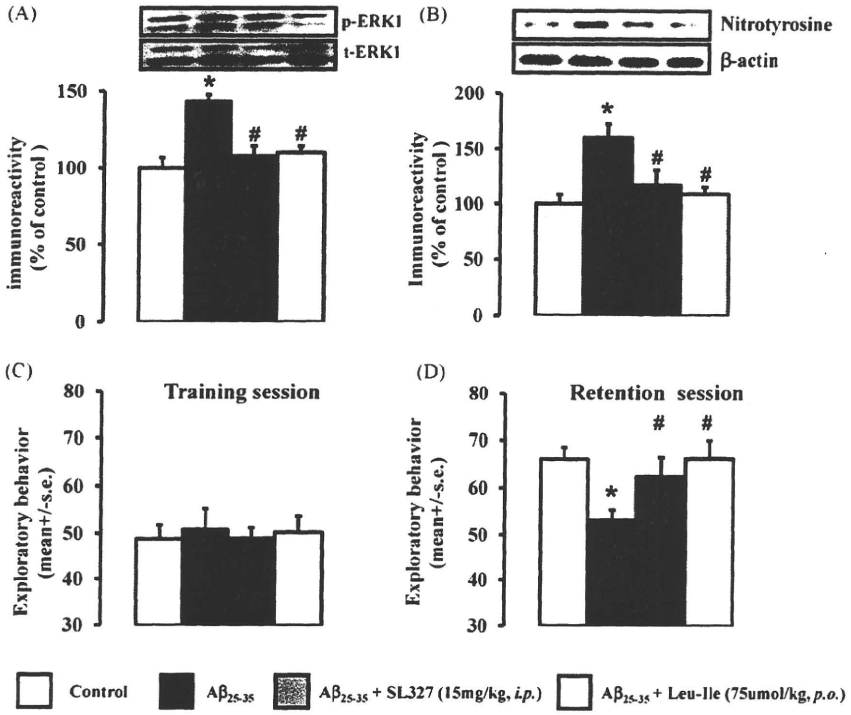

Fig. 4. Lue-Ile prevents the hyperphosphorylation of ERK induced by $A\beta_{25-35}$. (A and B) Sub-chronic treatment with SL327 or with Leu-Ile immediately before and 12 h after the *i.c.v.*-injection of $A\beta_{25-35}$ prevented the hyperphosphorylation of ERK (on Day 1), the enhanced nitration of protein (on Day 5) in the hippocampus and the impairment of memory (on Day 5) in mice. Data were presented as the mean ± S.E.; $n = 4$ for A and B, $n = 10$ for C and D. $^{*}p < 0.05$ vs. control. $^{\#}p < 0.05$ vs. $A\beta_{25-35}$. $A\beta_{25-35}$: Amyloid beta 25–35.

Leu-Ile immediately before and 12 h after the *i.c.v.*-injection of $A\beta_{25-35}$ were found to be same with those of SL327 (Fig. 4A–D) The results indicated that Leu-Ile protects the memory function in mice via restraining $A\beta_{25-35}$-induced hyperphosphorylation of ERK and resultant enhanced nitration of protein in the hippocampus.

4. Discussion

Providing a preventive alternative for the progressive cognitive decline in AD can improve the quality of lives of patients. In this study, we have provided one more alternative, a candidate of dietary supplement, for the prevention of Aβ-induced cognitive impairment. Oral administration of Leu-Ile protected against the nitration of proteins in the hippocampus and resultant impairment of memory in mice induced by $A\beta_{25-35}$ via regulating ERK.

In the early stage of AD pathology, the elevated levels of Aβ, phosphorylated ERK, and iNOS as well as peroxynitrite-mediated damage are associated with the progressive cognitive failure [28,45,46,55,59,62,65]. In their relationship, Aβ induces iNOS that mediates peroxynitrite damage via the hyperphosphorylation of ERK, while the selective inhibition of ERK or iNOS abolishes the neurotoxicity of Aβ [37,49].

Normally, ERK regulates a diverse array of functions through proper phosphorylation and dephosphorylation [60]. The transient enhancement in phosphorylation of ERK plays a critical role in the hippocampal synaptic plasticity as well as learning and memory [57]. The persistent increase in the phosphorylation of ERK is associated with the cell death [72] as well as the impairment of memory [14]. On the contrary, hypophosphorylation of ERK is also associated with the impairment of memory [70]. These diverse biological outcomes of ERK are decided by the physiological and pathological cellular environments as well as the cellular and subcellular localization of ERK [59]. The diversity and the accessibility of the potential substrates in the sub-cellular compartments also define the various cellular responses mediated by ERK [2].

The abnormal phosphorylation of ERK is persistently involved in the pathophysiology of AD. In the damaged areas of AD brain, the disease-stage-dependent abnormal phosphorylation of ERK is observed while the level of total ERK is not changed [29]. The hyperphosphorylation of ERK is found in the early stages of the pathological development of AD, while hypophosphorylation is found in the later stages [65]. The hyperphosphorylation of ERK mediates the neurotoxicity of Aβ [13,33,49] while the hypophosphorylation of ERK impairs the memory function [51,70]. At the early stage of exposure, Aβ generates hydrogen peroxide by reducing metal ions [21,56]. Aβ could also bind with catalase at a high affinity and inhibit the breakdown of hydrogen peroxide [34]. Scavenging of the hydrogen peroxide prevents the neurotoxicity of Aβ [6,8,27]. The hydrogen peroxide is global inducer of the hyperphosphorylation of ERK [25,36]. Further, the hyperphosphorylation of ERK is associated with the over-expression of iNOS [20,44,71] which elevates the level of nitric oxide in the cell and boosts the interaction of nitric oxide with superoxide to form prexoynitrite and the resultant nitration of protein [50]. The harmful outcome of the persistent hyperphosphorylation of ERK therefore could be due to the pathological environment that created by the elevated levels of hydrogen peroxide induced by Aβ [8,21,49].

The hyperphosphorylation of ERK mediates the cellular toxicity of 6-OHDA, a potent generator of hydrogen peroxide [19,23]. We have previously reported that Leu-Ile could protect against the cellular damage induced by 6-OHDA in mice [39]. In the present study, Leu-Ile prevented the hyperphosphorylation of ERK induced by $A\beta_{25-35}$. Whether or not Leu-Ile inhibits the production of hydrogen peroxide induced by $A\beta_{25-35}$ or scavenges hydrogen peroxide to prevent the hyperphosphorylation of ERK remains to be further studied.